Plant Soil
https://doi.org/10.1007/s11104-020-04714-x

REGULAR ARTICLE

Soil chemistry, elemental profiles and elemental distribution in nickel hyperaccumulator species from New Caledonia

Vidiro Gei · Guillaume Echevarria · Peter D. Erskine · Sandrine Isnard · Bruno Fogliani · Emmanuelle Montargès-Pelletier · Tanguy Jaffré · Kathryn M. Spiers · Jan Garrevoet · Antony van der Ent

Received: 6 May 2020 / Accepted: 8 September 2020

Abstract
Aims This study aimed to establish elemental profiles and to spatially resolve the elemental distribution in five New Caledonian woody Ni hyperaccumulator plant species (*Geissois pruinosa* var. *pruinosa*, *Homalium francii*, *Hybanthus austrocaledonicus*, *Psychotria gabriellae*, and *Pycnandra acuminata*) originating from the Cunoniaceae, Salicaceae, Violaceae, Rubiaceae, and Sapotaceae families respectively.
Methods Using synchrotron-based micro-X-ray Fluorescence (μXRF) imaging of different plant tissues, from the roots to the shoots and reproductive organs, this study aimed to clarify how distribution patterns of nickel, and other physiologically relevant elements, differ between these species.
Results The results show that the tissue-level and cellular-level distribution of nickel in *P. gabriellae, H. austrocaledonicus, G. pruinosa* var. *pruinosa,* and *H. francii* conform with the majority of studied Ni hyperaccumulator plant species globally, including (temperate) herbaceous species, with localization mainly in epidermal cells and phloem bundles. However,

Responsible Editor: Juan Barcelo.

Electronic supplementary material The online version of this article (https://doi.org/10.1007/s11104-020-04714-x) contains supplementary material, which is available to authorized users.

V. Gei · G. Echevarria · P. D. Erskine · A. van der Ent
Centre for Mined Land Rehabilitation, Sustainable Minerals Institute, The University of Queensland, Brisbane, Australia

G. Echevarria · A. van der Ent (✉)
Université de Lorraine – INRAE, Laboratoire Sols et Environnement, UMR 1120, Vandœuvre-lès-Nancy, France
e-mail: a.vanderent@uq.edu.au

S. Isnard · T. Jaffré
AMAP, Université de Montpellier, IRD, CIRAD, CNRS, INRAE, Montpellier, France

S. Isnard · T. Jaffré
AMAP, IRD, Herbier de Nouméa, Nouméa, New Caledonia

B. Fogliani
Institut Agronomique néo-Calédonien (IAC), Equipe ARBOREAL (AgricultuRe BiOdiveRsité Et vAlorisation), Noumea, New Caledonia

E. Montargès-Pelletier
Laboratoire Interdisciplinaire des Environnements Continentaux, CNRS, Université de Lorraine, Vandœuvre-lès-Nancy, France

K. M. Spiers · J. Garrevoet
Photon Science, Deutsches Elektronen-Synchrotron DESY, Hamburg, Germany

Published online: 15 October 2020

P. acuminata has nickel-rich laticifers, which constitute an independent network of cells that is parallel to the vascular bundles and are the main sink for nickel.
Conclusions Synchrotron-based micro-X-ray Fluorescence (μXRF) is a powerful method for investigating how metal hyperaccumulation influences acquisition and spatial distribution of a wide range of elements. This non-invasive method enables investigation into the in vivo distribution of multiple elements and the structure and organisation of cells (e.g. laticifers).

Keywords Hyperaccumulator · Elemental distribution · Latex · X-ray fluorescence microscopy

Introduction

Hyperaccumulators are unusual plants that accumulate particular metals or metalloids in their living tissues to levels that are 2–3 orders of magnitude greater than is normal for most plants growing on similar soils (van der Ent et al. 2012; Reeves et al. 2018a, 2018b). Nickel hyperaccumulator plants are defined as plants with Ni concentrations in leaves >1000 μg g^{-1} dry weight (Jaffré et al. 1976; Reeves 2003; van der Ent et al. 2013). Discovering hyperaccumulators and understanding their ecology could lead to identifying potential species to be utilized in novel phytotechnologies such as agromining or phytoextraction of valuable metals. They could be used in accumulating trace metals in naturally-mineralised agricultural soils, low grade ores, mine tailings, or mineral processing wastes (Chaney 1983; van der Ent et al. 2015a); and then harvested and processed to extract high-grade bio-ores or 'eco-catalysts' (Brooks et al. 1998; Brooks and Robinson 1998; Chaney et al. 2007; Losfeld et al. 2015b). Nickel phytomining is envisaged to become transformative in the rehabilitation of tropical laterite mining operations as part of rehabilitation strategies (van der Ent et al. 2013, 2015a; Losfeld et al. 2015a, 2015b; Erskine et al. 2018).

Currently, there are approximately 500 documented Ni hyperaccumulators worldwide (Reeves et al. 2018a). The majority of the Ni hyperaccumulators have been recorded in Brazil (130) (Reeves et al. 2007), Southern Europe and Minor Asia (80–90) (Brooks et al. 1979; Adıgüzel and Reeves 2012), New Caledonia (65) (Jaffré et al. 2013; van der Ent et al. 2015c), and Malaysia (24) (van der Ent et al. 2015a, 2015b, 2018c). Recent screening of herbarium samples using a portable XRF instrument in New Caledonia has revealed the existence of 99 Ni hyperaccumulators (65 known previously) and 74 Mn hyperaccumulators (11 known previously), meaning that more hyperaccumulators are to be discovered with such fast and non-destructive methods (Gei et al. 2018, 2020). One of the most unusual Ni hyperaccumulators is the tree *Pycnandra* (formerly *Sebertia*) *acuminata*, endemic to New Caledonia, whose latex contains up to 257 mg Ni g^{-1} dry latex (Jaffré et al. 1976; Jaffré et al. 2018). Hyperaccumulation is an extreme expression of transition element metabolic regulation in plants, which involves specific transporters and sequestration of metal ions and chelates in specific sink tissues (Krämer et al. 2007; Andresen et al. 2018). Hence, knowledge of the specific sequestering and transport mechanisms within these hyperaccumulating plants is crucial to better understand this phenomenon (van der Ent et al. 2017a, 2017b). The frequent occurrence of hyperaccumulation in a number of different clades suggests that Ni hyperaccumulation evolved repeatedly in different lineages (Pollard et al. 2002; Krämer 2010), but it is unknown whether physiological mechanisms of hyperaccumulation differ between the phylogenetic groups (i.e. whether non-related hyperaccumulating species have similar ecophysiological processes – inferred from cellular and tissue-level elemental distribution – associated with hyperaccumulation).

Our understanding of the diversity of Ni hyperaccumulation mechanisms is limited because studies on the spatial elemental distribution in tissues and cells have only been performed for less than 10% of the >500 Ni hyperaccumulating plant species known globally (Mesjasz-Przybyłowicz et al. 2016). Most of the studies initially conducted concerned small herbaceous plants from the families Brassicaceae, Asteraceae, and Celastraceae (e.g. *Alyssum* (now *Odontarrhena*), *Noccaea* (formerly *Thlaspi*), *Berkheya*, *Senecio,* and *Stackhousia*) and the leaves were typically the analysed parts, while stems and roots were less often investigated (Mesjasz-Przybyłowicz and Balkwill 1994; Mesjasz-Przybyłowicz et al. 1996a, b, 1997a, b, c, 2001a, b, 2007; Küpper et al. 2001; Bhatia et al. 2003, 2004; Broadhurst et al. 2004, 2009; McNear et al. 2005; Tappero et al. 2007). The only tropical woody shrub analysed was *Hybanthus floribundus* (Violaceae) for which Ni was mainly reported in the leaf epidermis (Bidwell et al. 2004; Kachenko et al. 2008). There is

also a short report on species from the genera *Phyllanthus* (Phyllanthaceae), *Euphorbia* and *Leucocroton* (Euphorbiaceae) from Cuba which reported that Ni concentration was highest in laticifers of all the species, which all had latex (Berazaín et al. 2007), but it confirmed that leaf epidermis was the storage location for all species studied. For the majority of investigated Ni hyperaccumulator plant species, Ni is a priori preferentially accumulated in foliar epidermal cells (Mesjasz-Przybyłowicz and Balkwill 1994; Mesjasz-Przybyłowicz et al., 1996a, b, 1997b, 1997c, 2001b; Küpper et al. 2001; Bidwell et al. 2004; Bhatia et al. 2004; Broadhurst et al. 2004) with the exception of *Berkheya coddii*, where Ni occurs at high concentrations in the palisade parenchyma (Groeber et al. 2015). The accumulation of Ni in leaf vacuoles in complexes with organic acids is often interpreted as a mechanism of metal detoxification and maintaining homeostasis (Seregin and Kozhevnikova 2006). Recently, several detailed studies on tropical woody shrubs and trees of the genera *Phyllanthus*, *Glochidion* (Phyllanthaceae), and *Rinorea* (Violaceae) have shed more light on cellular and sub-cellular distribution by using X-ray Fluorescence Microscopy (μXRF) and Proton Induced X-ray Emission (PIXE) techniques, by providing highly resolved mapping and low limits of detection (van der Ent et al. 2017a, 2017b, 2018b). These studies have shown that in phylogenetically distant species there is remarkably similar chemical form and distribution of Ni within plant organs and tissues.

This study is a comparative assessment of elemental concentrations and spatial distribution in distantly related species from New Caledonia to establish whether similar patterns of Ni hyperaccumulation mechanisms, observed so far globally, hold true for woody New Caledonian hyperaccumulator plants. Therefore, synchrotron μXRF was used to produce highly resolved elemental maps of different tissues in an array of species that occur in New Caledonia. The model plants analysed in this study were chosen to be as representative as possible of New Caledonian hyperaccumulator lineages (Fig. 1). The five selected species represent five families and four plant orders (Ericales, Gentianales, Malpighiales, Oxalidales) known to contain hyperaccumulator species worldwide. We aimed to investigate whether distribution patterns of Ni at the cellular and tissue level in the roots, stems, and leaves, and those of other physiologically relevant elements (e.g. Ca, K, Mn, Co, Zn), differ among these species.

Materials and methods

Species ecology

All five taxa (*Geissois pruinosa* var. *pruinosa*, *Homalium francii*, *Hybanthus austrocaledonicus*, *Psychotria gabriellae,* and *Pycnandra acuminata*) (Fig. 1) are endemic to New Caledonia and grow on soils derived from ultramafic bedrock. All of the taxa have a wide distribution in New Caledonia (Fig. 2). *Homalium francii*, *H. austrocaledonicus*, *P. gabriellae*, and *P. acuminata* occur in dense humid forest, the first three species being common understory shrubs, whereas the latter is an uncommon upper midstory to canopy tree (Swenson and Munzinger 2010). *Geissois pruinosa* is an ecologically ubiquitous species that occurs in maquis, most often in forest edges and sometimes in dense humid forests, however var. *pruinosa* is restricted to the southern part of New Caledonia (Jaffré et al. 1979; Hopkins et al. 2014). These taxa are ultramafic obligates, except for *Homalium francii* (Jaffré and Veillon 1990) and *Hybanthus austrocaledonicus* (Paul et al. 2020) which also occur on other types of soils.

Collection of plant samples and preparation

All species were collected in New Caledonia (Fig. 2) from natural populations in the Parc Provincial de la Rivière Bleue, except for *Geissois pruinosa* var. *pruinosa* which was collected at Monts des Koghis. Branch segments were collected from shrubs or obtained from the canopy of mature trees with a pole pruner, packed in moist paper and kept in sealed plastic bags, then brought to the PETRA III Synchrotron at DESY (Deutsches Elektronen-Synchrotron, Hamburg, Germany) in a fresh state. In addition, tissue samples were excised with a razor blade in the field and immediately shock-frozen using a metal mirror technique in which the samples were pressed between a block of copper (Cu)-metal cooled by liquid N_2 and a second cooled Cu-metal block attached to a Teflon holder. This ensured extremely fast freezing of the plant tissue samples to prevent cellular damage by ice crystal formation. The frozen samples were then wrapped in aluminium (Al) foil, transported and subsequently stored in a cryogenic container (at least −190 °C) until further processing (e.g. sectioning and mounting for μXRF analysis as described below).

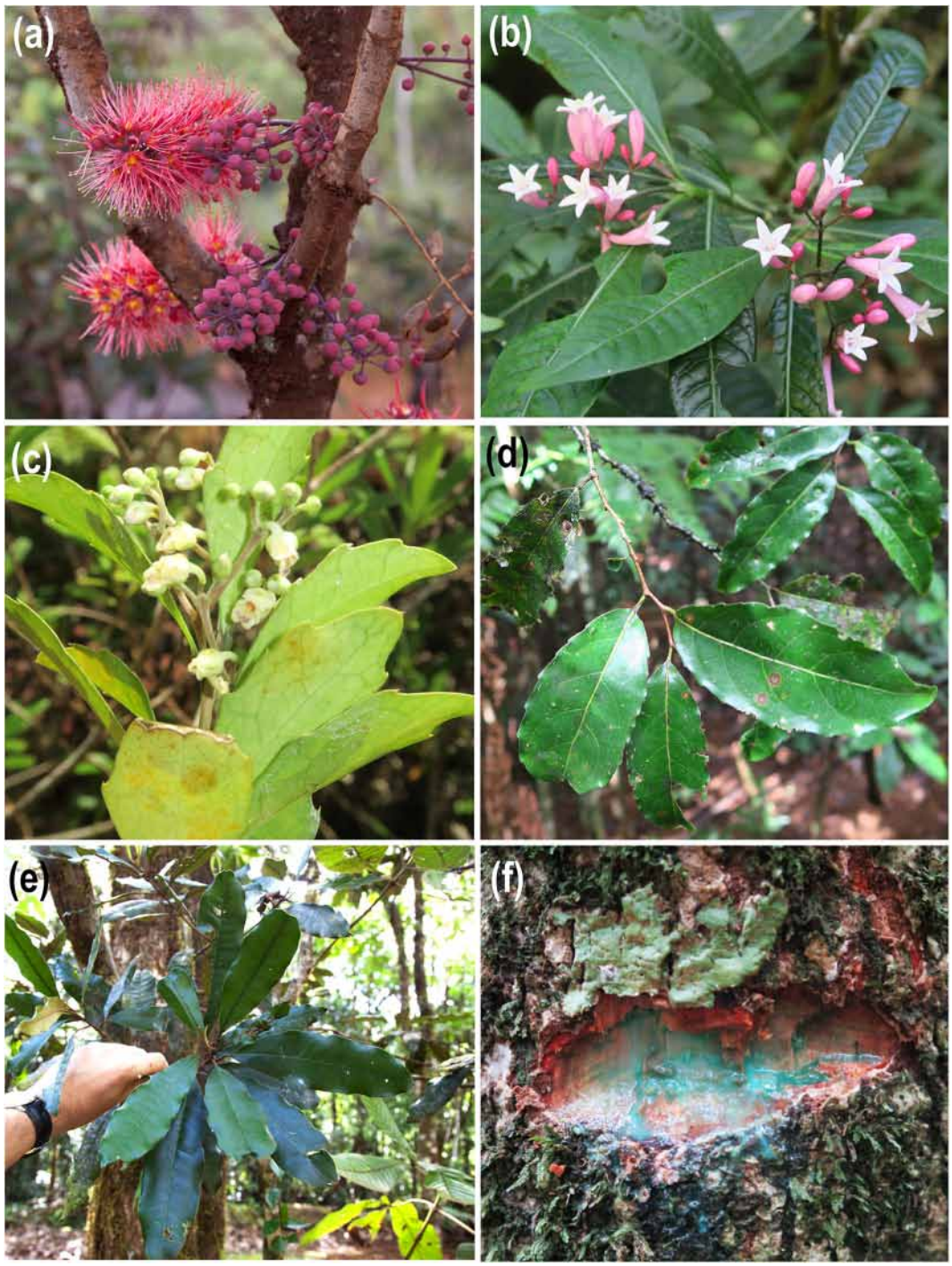

Fig. 1 *Geissois pruinosa* var. *pruinosa* (Cunoniaceae) cauliflorous inflorescences (**a**), *Psychotria gabriellae* (Rubiaceae) branch with leaves and inflorescences (**b**), *Hybanthus austrocaledonicus* (Violaceae) *branch* with leaves and inflorescence (**c**), *Homalium francii* (Salicaceae) branch with leaves (**d**), *Pycnandra acuminata* (Sapotaceae) branch with leaves **(e)**, and cut bark of stem exuding latex (**f**)

Freeze-dried specimens were prepared by sealing frozen samples in Ultralene film held onto XRF sample cups (polypropylene, 4 μm) with small holes punctured in the film for sublimed water to escape. The freeze-

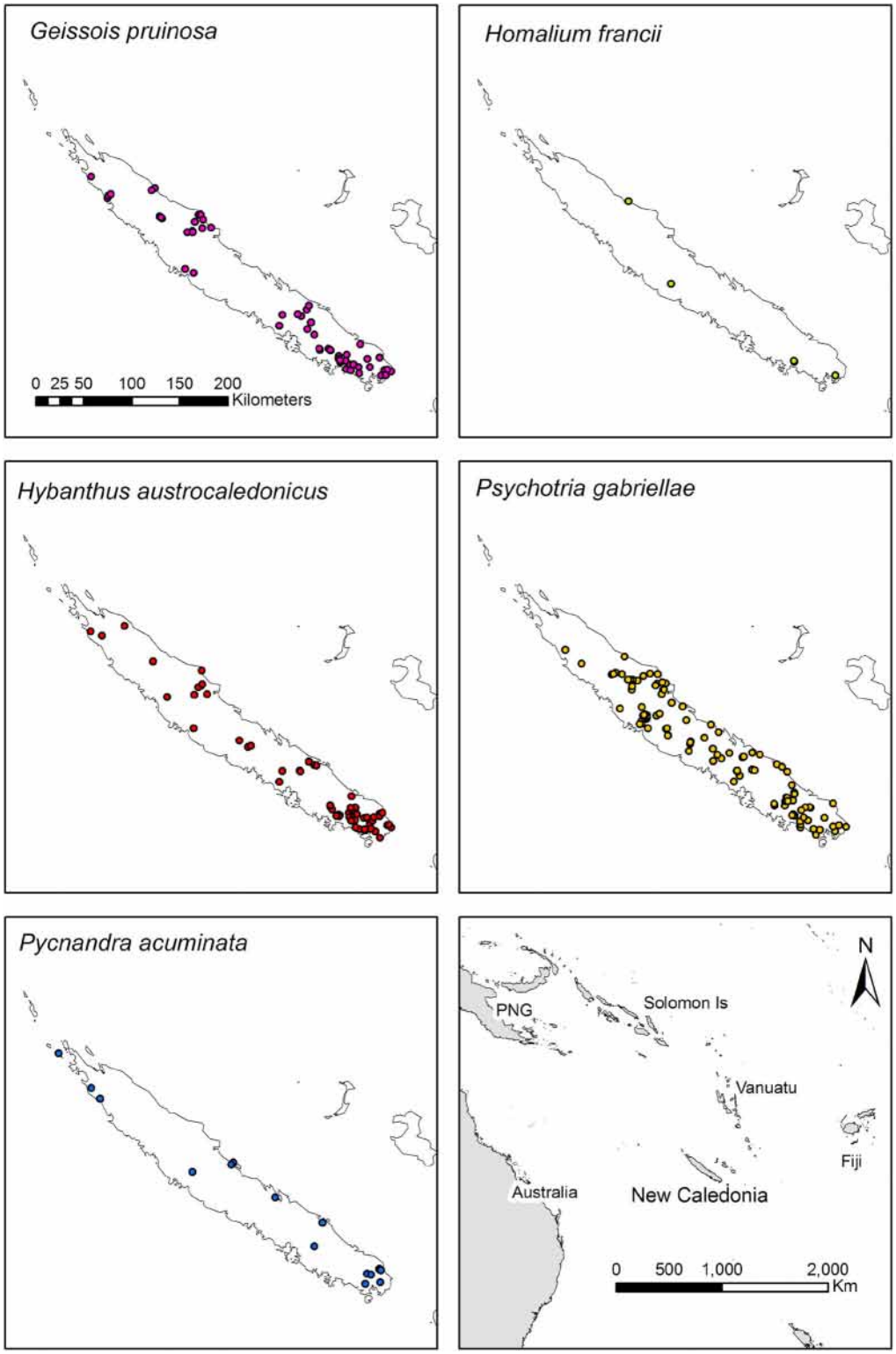

Fig. 2 Geographical distribution of *Geissois pruinosa* (all varieties), *Psychotria gabriellae*, *Homalium francii*, *Hybanthus austrocaledonicus* and *Pycnandra acuminata* in New Caledonia on the basis of herbarium (NOU) records. Map generated by ArcGIS (Esri)

Table 1 Habitat soil elemental concentrations in the natural habitats of *Geissois pruinosa* var. *pruinosa*, *Hybanthus austrocaledonicus*, *Psychotria gabriellae* and *Pycnandra acuminata*. The concentration values are ranges and means in μg g^{-1} or in mg g^{-1} when indicated with an asterisk* expressed on dry weight basis. The digests and extracts were analysed with ICP-AES. The 'total' is extractable with HCL/HNO_3 digest, 'DTPA' is extractable with Diethylenetriamine pentaacetic acid solution, and '$Sr(NO_3)_2$' is extractable with strontium nitrate solution. The *Homalium francii* samples were collected in close proximity of *Pycnandra acuminata*, therefore the soil habitat chemistry will be similar

Species	n	Habitat soil chemistry					
		pH	Mg (total)*	Al (total)*	P (total)	S (total)	K (total)
Geissois pruinosa var. *pruinosa*	3	6.1–6.2 [6.2]	15.2–20.1 [18.4]	12.2–14.6 [13.2]	278–305 [296]	585–959 [712]	233[α]
Hybanthus austrocaledonicus	1	5.9	7.2	34.9	295	648	–
Psychotria gabriellae	3	5.1–5.9 [5.4]	8.8–14.1 [11.9]	22.3–31.9 [28.1]	751–779 [765]	887–1200 [1080]	231–864 [627]
Pycnandra acuminata	1	5.8	5.2	42.5	373	716	224
Species	n	Ca (total)	Cr (total)*	Cr (DTPA)	Cr ($Sr(NO_3)_2$)	Mn (total)	Mn (DTPA)
Geissois pruinosa var. *pruinosa*	3	1270–1550 [1370]	6.7–8.0 [7.3]	0.3–0.5 [0.4]	0.1–0.3 [0.2]	4160–4320 [4230]	571–614 [594]
Hybanthus austrocaledonicus	1	1020	6.6	0.2	0.2	7080	842
Psychotria gabriellae	3	1370–3250 [2510]	1.8–12 [5.4]	0.5–1 [0.9]	0.2–0.7 [0.6]	2880–4670 [3540]	780–1090 [891]
Pycnandra acuminata	1	459	8.6	0.5	0.1	7280	875
Species	n	Mn ($Sr(NO_3)_2$)	Fe (total)*	Fe ($Sr(NO_3)_2$)	Co (total)	Co (DTPA)	Co ($Sr(NO_3)_2$)
Geissois pruinosa var. *pruinosa*	3	16.1–20.5 [18.1]	354–388 [366]	0.04–0.3 [0.2]	845–933 [875]	55.6–58.7 [57.1]	0.7–0.9 [0.8]
Hybanthus austrocaledonicus	1	30.6	289	0.1	952	48.6	0.4
Psychotria gabriellae	3	32.9–285 [181]	128–375 [217]	0.1–16 [9.7]	339–638 [445]	71.3–77.8 [75.4]	0.7–8 [5]
Pycnandra acuminata	1	105	346	0.2	1080	65.5	1.3
Species	n	Ni (total)*	Ni (DTPA)	Ni ($Sr(NO_3)_2$)	Zn (total)	Zn (DTPA)	Zn ($Sr(NO_3)_2$)
Geissois pruinosa var. *pruinosa*	3	9.9–10.5 [10.2]	320–426 [367]	6.4–8.2 [7.1]	324–345 [336]	13.1–15.5 [13.9]	0.3–0.4 [0.3]
Hybanthus austrocaledonicus	1	7.9	627	18.2	287	10.5	0.3
Psychotria gabriellae	3	2.7–5.7 [3.7]	300–443 [352]	8.4–26.3 [18.9]	204–322 [250]	7.5–67.5 [46.1]	0.4–4.1 [2.8]
Pycnandra acuminata	1	8.3	599	38	321	9.8	0.9

[α] Only one sample, * ranges and means in mg g^{-1}, n = number of analysed samples

drying process started at −196 °C by inserting the framed frozen samples onto a large steel block cooled in liquid nitrogen. The cooled block with samples was then loaded into the freeze-drying machine (Thermoline) and vacuum-pumped and set to −85 °C. Freeze-drying then progressed very slowly (by changing the set temperature with 5 °C increments) over the course of four days until room temperature was reached.

Light microscopy and histochemistry

Plant tissue samples were fixed in 3% glutaraldehyde upon collection. Sections of 50–100 μm thickness were obtained with a vibratome (Leica VTS1000) after embedding in agarose and stained with 1% toluidine blue to reveal anatomical features to assist in the interpretation of the element maps (Supporting Information Fig. S1 and S2).

Soil sampling and determination of chemical properties

Soil samples were taken from near the base of each plant from which the tissue samples were also collected in the Parc Provincial de la Rivière Bleue (Table 1). In total three soil samples were collected for *G. pruinosa* var. *pruinosa*, three for *P. gabriellae,* one for *H. austrocaledonicus* and one for *Pycnandra acuminata*. *Homalium francii* was collected very close to the *P. acuminata* so the habitat elemental concentration values would be similar, hence no sample was collected. The soil samples were taken with a plastic scoop from a depth of 10–20 cm. These soil samples were air-dried and sieved (<2 mm). Sub-samples (~300 mg) were digested using 9 mL 70% HNO_3 and 3 mL 37% HCl per sample in a microwave digester (Milestone Start D) for 1.5 h and diluted to 40 mL with ultrapure water before analysis to obtain pseudo-total elemental concentrations. Soil pH was measured in a 1:2.5 soil:water mixture after 2 h of shaking. Exchangeable trace elements were extracted in 0.1 M $Sr(NO_3)_2$ at a soil:solution ratio of 1:4 (10 g soil with 40 ml solution) and 2 h shaking time (adapted from Kukier and Chaney 2001). As a means of estimating potentially phytoavailable trace elements, diethylenetriamine penta-acetic acid (DTPA-extractant) was used according to the method of Becquer et al. (1995) which was adapted from the original method by Lindsay and Norvell (1978), with the following modifications: exclusion of triethanolamine (TEA), pH adjusted to 5.3, 5 g soil used with 25 mL extractant to prevent saturation of the DTPA, and an extraction time of 1 h.

Chemical analysis of bulk tissue samples and soil extracts

Plant tissue samples (leaves, bark, branches, roots, fruits, flowers) for bulk chemical analysis were collected in the field from the same plants. Latex was collected by cutting the bark of *P. acuminata*. These samples were dried at 70 °C for five days in a drying oven. The dried plant tissue samples were subsequently ground and digested using 4 ml HNO_3 (70%) in a microwave oven (Milestone Start D) for a 45-min programme and diluted to 30 mL with ultrapure water (Millipore 18.2 MΩ·cm at 25 °C) before analysis with ICP-AES (Varian Vista Pro II) for Ni, Co, Cr, Cu, Zn, Mn, Fe, Mg, Ca, Na, K, S, and P. Soil extracts were also analysed using ICP-AES for the same elements. In-line internal addition standardization using yttrium was used to compensate for matrix-based effects.

X-ray fluorescence microscopy (μXRF)

The X-ray fluorescence microscopy experiment was undertaken at Beamline P06 at the PETRA III (Deutsches Elektronen-Synchrotron; DESY, Hamburg, Germany), a 6 GeV 3rd Generation Synchrotron Radiation Source. The undulator beam was monochromatised with a cryogenically cooled Si(111) channel-cut monochromator to an energy of 12 keV with a flux of ~1.1×10^{10} photon/s. A Kirkpatrick-Baez mirror pair was used to focus the incident beam to 700 × 530 nm (hor × ver). The Maia detector uses a large detector array in backscatter geometry to maximize detected signal and count-rates for efficient imaging. Maia enables high overall count-rates and uses an annular detector geometry, where the beam passes though the detector and strikes the sample at normal incidence (Kirkham et al. 2010; Siddons et al. 2014). This enables a large solid-angle (~1.2 sr) to be achieved in order to either maximize detected signal or to reduce the dose and potential damage to a specimen (Ryan et al. 2010, 2014). We first conducted a quick 'survey scan' (50–100 μm with a dwell time of 1–2 ms, taking 5–10 min. in total) to select the precise scan area. Then a 'detailed scan' was conducted (resolution of 2–10 μm and a dwell time of 8–20 ms, taking 60–180 min. in total).

Table 2 Bulk macro-elemental concentrations of various plant parts of *Geissois pruinosa* var. *pruinosa, Homalium francii, Hybanthus austrocaledonicus, Psychotria gabriellae,* and *Pycnandra acuminata.* The concentration values are ranges and means in μg g^{-1} or in mg g^{-1} when indicated with an asterisk* expressed on dry weight basis. Hash# indicates sample size if different from the n. The acid digests were analysed with ICP-AES

Species	n	Ca*	Fe	K*	Mg*	Na	P	S*
Leaves								
Geissois pruinosa var. *pruinosa*	12	2.97–4.7 [3.91]	10–46 [29]	1.09–1.83 [1.35]	1.83–5.17 [4.16]	220–740 [400]	92–490 [270]; 11#	0.51–8.32 [1.87]
Homalium francii	12	1.24–3.61 [2.02]	37–300 [140]	1.17–10.4 [5.84]	1.2–3.33 [2.27]	130–3090 [1810]	160–1460 [580]	0.85–3.48 [2.02]
Hybanthus austrocaledonicus	10	1.16–2.29 [1.71]	31–71 [47]	1.83–10.200 [6.28]	2.76–4.9 [3.4]	730–6000 [2400]	7–680 [360]; 8#	1.14–3.82 [2.75]
Psychotria gabriellae	12	1.40–5.17 [2.82]	19–1510 [170]	0.48–19.0 [3.09]	0.91–2.93 [1.6]	390–2180 [950]	140–860 [480]; 10#	0.75–5.27 [2.94]
Pycnandra acuminata	12	0.66–5.62 [1.23]	26–340 [81]	3.3–7.74 [5.20]	0.51–1.85 [0.98]	1130–2590 [1580]	55–810 [290]	0.51–1.93 [1.17]
Branches								
Geissois pruinosa var. *pruinosa*	3	0.84–5.26 [3.47]	7.7–12 [9.2]	0.44–1.89 [1.05]	0.51–1.8 [1.04]	140–330 [230]	110–600 [330]	0.33–0.75 [0.480]
Homalium francii	3	3.67–5.46 [4.36]	63–76 [71]	1.3–2.56 [1.74]	0.55–1.13 [0.91]	160–190 [170]	87–220 [140]	0.36–0.71 [0.52]
Hybanthus austrocaledonicus	2	1.66–1.70 [1.68]	7–15 [11]	2.19–2.97 [2.58]	0.44–0.8 [0.62]	610–670 [640]	130–170 [150]	0.47–0.73 [0.6]
Psychotria gabriellae	4	2.26–4.68 [3.01]	15–45 [26]	2.65–4.47 [3.39]	0.23–0.61 [0.35]	270–2710 [1150]	69–160 [110]	0.52–0.7 [0.59]
Pycnandra acuminata	2	1.55–4.26 [2.90]	180–1030 [610]	1.77–4.38 [3.07]	0.43–2.44 [1.44]	1600–1850 [1720]	340–740 [540]	0.72–1.04 [0.88]
Bark								
Geissois pruinosa var. *pruinosa*	1	16.3	9.1	0.61	2.11	75	100	0.81
Homalium francii	1	24.8	15	2.56	0.24	37	170	0.74
Hybanthus austrocaledonicus	4	0.93–1.44 [1.17]	15–240 [82]	7.69–8.88 [8.38]	0.37–0.74 [0.52]	21–350 [150]	93–220 [170]	0.76–2.47 [1.38]
Pycnandra acuminata	2	0.6–5.28 [2.94]	21–22 [22]	0.43–0.49 [0.46]	0.07–0.0199 [0.09]	840–3780 [2310]	51–82 [66]	0.3–1.0 [0.65]
Roots								
Homalium francii	1	2.13	5710	1950	1.92	1920	240	0.71
Hybanthus austrocaledonicus	2	0.77–5.13 [2.95]	870–1620 [1250]	2.41–2.46 [2.44]	0.53–1.73 [1.13]	53–390 [220]	140–220 [180]	0.74–0.97 [0.85]
Psychotria gabriellae	2	0.26–6.43 [3.35]	1080–2870 [1970]	1.51–1.73 [1.62]	0.34–1.17 [0.75]	930–1430 [1180]	160–2310 [1240]	0.76–0.81 [0.79]
Flowers								
Geissois pruinosa var. *pruinosa*	2	3.56–5.18 [4.37]	15–15 [15]	5.09–7.35 [6.22]	2.58–3.43 [3.0]	210–1040 [620]	530–860 [700]	1.14–1.75 [1.44]
Psychotria gabriellae	2	3.76–3.88 [3.82]	28–38 [33]	9.57–9.58 [9.57]	1.94–2.48 [2.21]	180–640 [410]	740–760 [750]	0.59–2.04 [1.31]
Fruits (pericarp except for *P. gabriellae*)								
Geissois pruinosa var. *pruinosa*	1	2.47	11	4.14	1.64	940	730	0.87
Psychotria gabriellae	3	2.05–5.92 [3.94]	12–17 [15]	7.15–8.5 [7.82]	1.9–2.15 [2.03]	240–390 [310]	610–950 [760]	1.47–1.66 [1.59]
Pycnandra acuminata	2	0.91–2.48 [1.7]	14–20 [17]	4.39–4.81 [4.600]	0.63–2.18 [1.41]	680–1180 [930]	200–680 [440]	0.67–0.91 [0.79]
Seeds (with endocarp in *P. gabriellae*)								
Psychotria gabriellae	1	2.1	13	2.44	1.5	54	1000	1.39

Table 2 (continued)

Species	n	Ca*	Fe	K*	Mg*	Na	P	S*
Pycnandra acuminata Latex	1	0.78	9.8	2.69	0.74	830	560	0.43
Pycnandra acuminata	2	7.46–17.04 [12.25]	61–200 [130]	1.14–3.8 [2.47]	0.48–1.36 [0.92]	1560–3320 [2440]	310–570 [440]	0.7–1.19 [0.94]

The live samples were prepared on-site immediately prior to scanning at beamline P06. The samples were hand cut with a stainless-steel razor blade ('dry knife') and analysed within 10 min after excision. The fresh and freeze-dried samples were mounted between two sheets of Ultralene thin film (4 μm) stretched over a Perspex frame magnetically attached to the horizontal-vertical motion stage at atmospheric temperature (~20 °C). The possibility of radiation-induced damage in μXRF analysis (especially in fresh/hydrated samples) is an important consideration that may limit the information sought from the analysis (van der Ent et al. 2017b). In a recent study, radiation dose limits for μXRF analysis were assessed, and in hydrated plant tissue dose-limits are 4.1 kGy before detectable damage occurs (Jones et al. 2019). To limit radiation damage, we used a fast scanning (per-pixel dwell time less than 20 ms so that effective radiation dose is low).

Data processing and statistics

The XRF event stream was analysed using the Dynamic Analysis method (Ryan and Jamieson 1993; Ryan 2000) as implemented in GeoPIXE (Ryan et al. 1990, 2005). The matrix file used for the spectra fitting was an assumed freeze-dried plant material composition of $C_{31}O_{15}H_{51}N_2S_{0.8}$ with a density of 0.75 g cm^{-3}, and for live/fresh samples the composition was $C_{7.3}O_{33}H_{59}N_{0.7}S_{0.8}$ with a density of 0.90 g cm^{-3} and considering two layers of Ultralene (4 μm).

Results

Soil chemistry in the habitat of the five species

Most of the soils originated from non- (Rivière-Bleue) or only partly serpentinised (Monts des Koghis) peridotite and were moderately weathered (i.e. they have full or partial ferralitic properties). The range of soil pH values was narrow around pH 6.0 (pH 5.8–6.2) except for the soils hosting *Psychotria gabriellae*, which were more acidic (< pH 5.5) than the other soils (Table 1). Total Fe ranged from 128 to 388 mg Fe g^{-1} with most around 300 mg Fe g^{-1} and total Al from 12.2–42.5 mg Al g^{-1}. Soils had high Mg concentrations from 5.2–20.1 mg Mg g^{-1} and depleted concentrations of Ca. All soils were extremely depleted in total K with most values around 200 μg K g^{-1} and none exceeded

Table 3 Bulk trace elemental concentrations of various plant parts of *Geissois pruinosa* var. *pruinosa, Homalium francii, Hybanthus austrocaledonicus, Psychotria gabriellae,* and *Pycnandra acuminata*. The concentration values are ranges and means in μg g^{-1} or in mg g^{-1} when indicated with an asterisk* expressed on dry weight basis. Hash# indicates sample size if different from the n. The acid digests were analysed with ICP-AES

Species	n	Al	Co	Cr	Cu	Mn	Ni*	Zn
Leaves								
Geissois pruinosa var. *pruinosa*	12	9.3–62 [42]	0.5–55 [39]	3.4–78 [56]	1.9–7.4 [2.3]	56–180 [93]	3.21–10.6 [8.99]	25–57 [39]
Homalium francii	12	11–230 [100]	0.1–120 [28]	4–120 [39]	5.1–29 [12]	24–76 [45]	2.65–9.48 [5.4]	26–220 [110]
Hybanthus austrocaledonicus	10	57–97 [75]	1.8–130 [30]; 9#	5.9–81 [38]; 7#	1.3–9.8 [6.6]	77–180 [120]	9.22–15.6 [12.7]	48–260 [100]
Psychotria gabriellae	12	20–160 [90]	3.2–90 [37]; 10#	1.2–51 [27]; 9#	3–36 [12]; 11#	22–140 [72]	10.2–32.200 [21.4]	14–200 [95]
Pycnandra acuminata	12	16–170 [69]	0.3–73 [18]	2.2–41 [19]; 9#	0.1–9.7 [2.4]	21–51 [28]	6.71–17.9 [13.3]	23–94 [50]
Branches								
Geissois pruinosa var. *pruinosa*	3	5.6–7.7 [6.5]	2.3–12 [5.7]	0.7–1.8 [1.3]	3.1–21 [9.9]	9.7–22 [15]	0.47–1.07 [0.72]	24–56 [39]
Homalium francii	3	16–19 [18]	0.2–1.7 [0.9]	2.7–2.9 [1.2]	1–8.4 [1.4]	8.8–17 [14]	0.87–0.95 [0.92]	20–25 [22]
Hybanthus austrocaledonicus	2	4.9–6.1 [2.3]	0.1–0.9 [0.5]	0.5–1.7 [1.1]	1.3–1.6 [1.5]	21–25 [23]	2.03–2.34 [2.18]	13–14 [14]
Psychotria gabriellae	4	6–22 [12]	0.5–2.8 [2]	1.1–3.3 [2]	2.6–4.7 [3.9]	14–73 [35]	4.61–14.6 [8.12]	22–53 [33]
Pycnandra acuminata	2	29–130 [82]	0.3–0.4 [0.3]	0.9–31 [16]	3.2–9.4 [6.3]	23–64 [44]	2.82–6.86 [4.84]	25–32 [28]
Bark								
Geissois pruinosa var. *pruinosa*	1	11	6.3	1.3	2.6	25	0.41	24
Homalium francii	1	21	2	0.6	0.5	20	0.92	45
Hybanthus austrocaledonicus	4	8.8–17 [13]	0.5–6.2 [3.3]	5.7–69 [30]	0.3–3 [1.5]	55–170 [130]	7.59–48.5 [26400]	39–170 [97]
Pycnandra acuminata	2	7.9–13 [10]	0.03–0.3 [0.2]	1.4–2.7 [1.3]	1.8–2.3 [2.1]	5.2–65 [35]	7.99–10.6 [9290]	35–50 [42]
Roots								
Homalium francii	1	740	0.2	140	9.1	110	1.24	36
Hybanthus austrocaledonicus	2	68–250 [160]	0.04–2.2 [1.1]	16–43 [30]	1.6–1.9 [1.7]	120–130 [120]	2.42–3.41 [2.91]	19–22 [21]
Psychotria gabriellae	2	120–160 [140]	0.6–3 [1.8]	25–35 [30]	4–7.2 [5.6]	58–170 [120]	2.2–2.83 [2.51]	14–16 [15]
Flowers								
Geissois pruinosa var. *pruinosa*	2	7–9.2 [8.1]	7–16 [12]	2.1–3.9 [1.3]	11–17 [14]	28–65 [47]	2.71–3.4 [3.06]	18–32 [25]
Psychotria gabriellae	2	27–60 [44]	0.4–11 [5.8]	0.1–16 [8.1]	4.6–6.3 [5.5]	34–150 [91]	14.51–18. 0 [16.3]	43–61 [52]
Fruits (pericarp except for *P. gabriellae*)								
Geissois pruinosa var. *pruinosa*	1	5.4	5.2	1.9	11	24	1.51	12
Psychotria gabriellae	3	6.7–19 [12]	0.9–1.6 [1.1]	1.5–7.6 [2.2]	5.2–6 [5.6]	20–25 [22]	8.66–11.3 [9.81]	29–34 [31]
Pycnandra acuminata	2	5.5–6.8 [6.2]	0.03–1 [0.5]	0.4–1.8 [1.1]	3.6–5.8 [2.6]	10–30 [20]	3.68–8.59 [6.13]	13–35 [24]
Seeds (with endocarp in *P. gabriellae*)								
Psychotria gabriellae	1	7.2	0.2	1.4	6.1	54	5.42	20

Table 3 (continued)

Species	n	Al	Co	Cr	Cu	Mn	Ni*	Zn
Pycnandra acuminata Latex	1	7.1	–	4.7	1.3	22	4.11	14
Pycnandra acuminata	2	120–1500 [810]	24–59 [41]	1.9–6.7 [4.3]	2.9–49 [26]	220–340 [280]	110–154 [132]	670–920 [800]

1000 μg K g^{-1}. Furthermore, P total concentrations were very low (from 280 to 780 μg P g^{-1}), as were S total concentrations (590–1200 μg S g^{-1}). Total Co, Cr, Mn, and Ni concentrations reflected typical values from ferralic ultramafic soils: 340–1080 μg Co g^{-1}, 339–1080 μg Cr g^{-1}, 2880–7280 μg Mn g^{-1}, and 2.7–10.5 mg Ni g^{-1} (Table 1).

Metal availability was assessed by both $Sr(NO_3)_2$ and DTPA extractions (Table 1). The former provides a good picture of exchangeable ions retained by the soil Cation Exchange Capacity (CEC), whereas DTPA extracts the isotopically-exchangeable pool, i.e. the Ni pool that supplies hyperaccumulators and non-hyperaccumulators (Echevarria et al. 1998, 2006; Massoura et al. 2005; Estrade et al. 2015). The $Sr(NO_3)_2$ exchangeable Ni in all soils ranged from 6.4–38 μg Ni g−1. Moreover, DTPA-extractable Ni was very high in all sampled soils. It varied from 300 to 627 μg Ni g^{-1} with no apparent difference between the plant species. One soil (*P. gabriellae* from Monts des Koghis) had exchangeable Co that was remarkably high (i.e. 8 μg Co g^{-1}) and exchangeable Mn was also highly available (i.e. 285 μg Mn g^{-1}). In the case of DTPA-extractable Co, it was noticeable that most of the soils had similar concentrations, limited between 49 and 78 μg Co g^{-1}; which appears higher than in typical ultramafic soils (Echevarria 2018; van der Ent et al. 2018a). For other metals, exchangeable concentrations were relatively low in all soils and within expected values.

Elemental profiles of the five species

Bulk elemental concentrations of major trace elements were obtained for different parts of the plant for the five taxa (Tables 2 and 3) and described below.

Roots It is not practically possible to entirely clean roots from soil particle contamination. Soil particles, and in particular nanometric or submicrometric particles, may be embedded and cannot be entirely removed by rigorous washing or brushing. However, some elements which are very unlikely to be taken up in large quantities by roots (e.g. Cr, Fe) help to detect soil contamination. Typically, K was low in the roots (<2460 μg K g^{-1}) and preferentially transferred in the leaves: all three species contained more than 1 Wt.% K in leaves. A similar pattern was seen for Ni with highly enhanced translocation to the leaves: (<3.41 mg Ni g^{-1} in roots of all three species whereas it reached 3.2 mg Ni g^{-1} in leaves).

Bark In the bark samples of *G. pruinosa* var. *pruinosa* and *H. francii*, Ca was extremely enriched (16 and 25 mg Ca g^{-1} respectively), whereas for *H. austrocaledonicus* and *P. acuminata*, Ca content was in the same range as in all other parts. The bark (including phloem) had very high concentrations of Ni in *H. austrocaledonicus* (up to 48.5 mg Ni g^{-1}), and in *P. acuminata* (up to 10 mg Ni g^{-1}). On the contrary, *G. pruinosa* var. *pruinosa* and *H. francii* had very low Ni concentrations (410 and 920 μg Ni g^{-1} respectively) in the bark.

Stem tissues (without bark) Similarly to the bark, Ni concentrations were low in the branches of both *G. pruinosa* var. *pruinosa* and *H. francii*. They were intermediate in *H. austrocaledonicus* and *P. acuminata* and high in *P. gabriellae* (>15 mg Ni g^{-1}) (data not shown).

Leaf tissues (whole leaf) Foliar Ca concentrations (Table 2) were typically five-fold higher than in the soils, in contrast to the extremely high soil Mg concentrations that had been effectively limited from uptake. All species except *G. pruinosa* var. *pruinosa* reached extremely high K concentrations in leaves (sometimes >10 mg K g^{-1}) in comparison to soil concentrations ranging from 224 to 864 μg K g^{-1} (Table 1). The maximum foliar K concentration for *G. pruinosa* var. *pruinosa* remained in the lower range compared to other species (Table 2), but it was still five times more than the total K in the soil. Even though soil S concentrations were low (<1200 μg S g^{-1}), foliar concentrations were remarkably high reaching up to 8320 μg S g^{-1} in the leaves. All five species are hypernickelophores (although the maximum value in this study for *Homalium francii* was 9480 μg Ni g^{-1}) (Table 3, Fig. 3), and Ni concentration values were consistent with earlier reports for these species (Jaffré and Schmid 1974; Reeves 2003; Jaffré et al. 2013). Although Co foliar concentrations were highly variable for a given species, *H. francii* and *H. austrocaledonicus* reached values ≥120 μg Co g^{-1}. Manganese concentrations of the five species in leaves were comparatively low (28–120 μg Mn g^{-1}), given the high available Mn concentrations in the soils (571–1090 μg Mn g^{-1} DTPA-extractable Mn).

Reproductive organs (flowers, fruits and seeds) Flowers of *P. gabriellae* were highly enriched in Ni, contrary to those of *G. pruinosa* var. *pruinosa* (Table 3). The fruits (i.e. pericarp, except for *P. gabriellae* as the endocarp surround the seed) were also strongly enriched in Ni in both *P. acuminata* (mean of 6130 μg Ni g^{-1}) and *P. gabriellae* (mean of 9810 μg Ni g^{-1}) but relatively low in *G. pruinosa* var. *pruinosa* (1510 μg Ni g^{-1}). Concentrations of other transition metals (i.e. Co, Cr, Mn, Zn) in fruits were remarkably low in comparison with those of Ni. Seeds of *P. acuminata* (seed *stricto* sensu) and *P. gabriellae* (seed *stricto* sensu surrounded by the endocarp i.e. pyrene) contained less Ni than the fruits (or flowers in case of *P. gabriellae*), with high range values (4110 and 5420 μg Ni g^{-1} respectively). The mesocarp of *P. acuminata* exuded green latex when sliced, suggesting high Ni concentrations in this seed.

Latex of Pycnandra acuminata Samples of latex collected from the trunks of *P. acuminata* in Rivière Bleue had a bright turquoise colour (Fig. 1f). The latex contained noticeable concentrations of Ca that exceeded 10 mg Ca g^{-1} and were always more than 10 times higher than Mg concentrations (Table 2). It contained some K (1140–3800 μg K g^{-1}) and Na (1560–3320 μg Na g^{-1}), with all other major elements showing concentrations below 1200 μg g^{-1}. It contained surprisingly high concentrations of Al (mean concentration of 810 μg Al g^{-1} with one value around 1500 μg Al g^{-1}) and Zn (mean concentration of 800 μg Zn g^{-1}). As expected (Sagner et al. 1998; Perrier et al. 2004; Schaumlöffel et al. 2003; Callahan et al. 2008), Ni concentrations were extremely high and ranged from 110 to 150 mg Ni g^{-1}. However, Co concentrations in the latex were relatively low (mean of 41 μg Co g^{-1}) compared to Ni concentrations. The Ni/Co ratio in latex was approximately 325, whereas it was approximately 10 in the soil DTPA extract.

Elemental distribution in whole leaf fragments Potassium was highly concentrated in the midrib of all species except for *P. gabriellae* (Fig. 4). It was also localised in the secondary veins for *H. austrocaledonicus* and *G. pruinosa* var. *pruinosa* and had a high background concentration throughout the leaves of *H. austrocaledonicus* but not in *G. pruinosa* var. *pruinosa*. In *P. gabriellae* there was a strong enrichment of K in minor veins whilst in *H. francii* K was enriched in the lamina surrounding the secondary veins. In contrast, K was depleted in the area surrounding the midrib of *P. acuminata*, but was

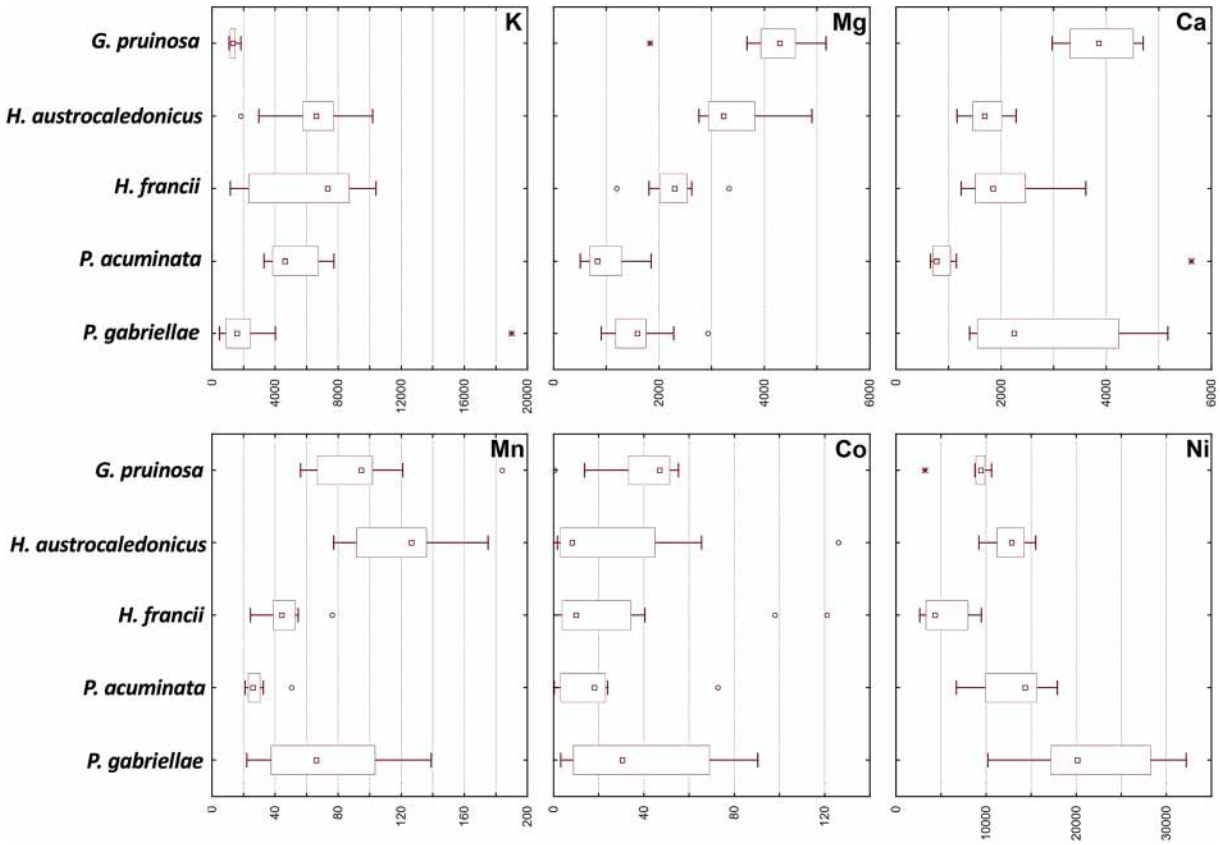

Fig. 3 Boxplots of the foliar concentrations of K, Mg, Ca and Mn, Co*, Ni in *Geissois pruinosa* var. *pruinosa* (*n* = 12), *Psychotria gabriellae* (n = 12, **n* = 10), *Homalium francii* (n = 12), *Hybanthus austrocaledonicus* (n = 10; **n* = 9) and *Pycnandra acuminata* (n = 12). Boxplots show ranges, medians, percentiles and outliers. All values in μg g^{-1} dry weight

somewhat enriched at the base of the secondary veins and depleted towards the outer ends.

There was no notable enrichment of Ca in the leaves of *P. gabriellae* (Fig. 4). In the other species Ca was mainly concentrated in major veins and appears as small Ca-oxalate crystals (micrometric cubes). In *G. pruinosa* var. *pruinosa* and *P. acuminata* these crystals underlined the structure of minor veins order; whereas in *H. austrocaledonicus* and *H. francii* they were more scattered throughout the leaf blade. Calcium was totally absent in the veins of *H. austrocaledonicus* but homogeneously distributed throughout the leaf blade.

In all species, Ni was strongly concentrated in the midveins and secondary veins except for *P. acuminata*, where Ni was concentrated in laticifers (Fig. 5). In *H. austrocaledonicus* and in *G. pruinosa* var. *pruinosa* Ni was also highly concentrated in the minor veins. That was not the case for *H. francii* and *P. gabriellae*, for the latter there was also a notable enrichment of Ni in the immediate surroundings of the main veins. In *P. acuminata*, Ni had a peculiar distribution –it was mainly distributed along a network of elongated cellular structures (laticifers) that were not part of the vascular system, unlike Ca or K that clearly highlight the vascular system. Manganese was co-localized with Ni in the veins of *H. francii*, but it had a different distribution than Ni in *G. pruinosa* var. *pruinosa* (Fig. 5) as it was mainly localised in the midrib and absent from all secondary and minor veins in this species. It was, however, highly enriched in the surrounding areas of the midrib and the secondary vein. Cobalt in *H. austrocaledonicus* and *P. acuminata* is co-localized with Ni throughout the leaf, although at much lower concentrations.

Images and anatomical sections of the actual scanned freeze-dried samples are provided in Suppl. Info (Figs. 4, 5). It should be noted that the concentrations of all elements appeared higher in the midvein and leaf margins (that are curved inwards in *H. austrocaledonicus*) due to greater thickness of these regions (hence generating more fluorescent X-rays from the greater mass). To a

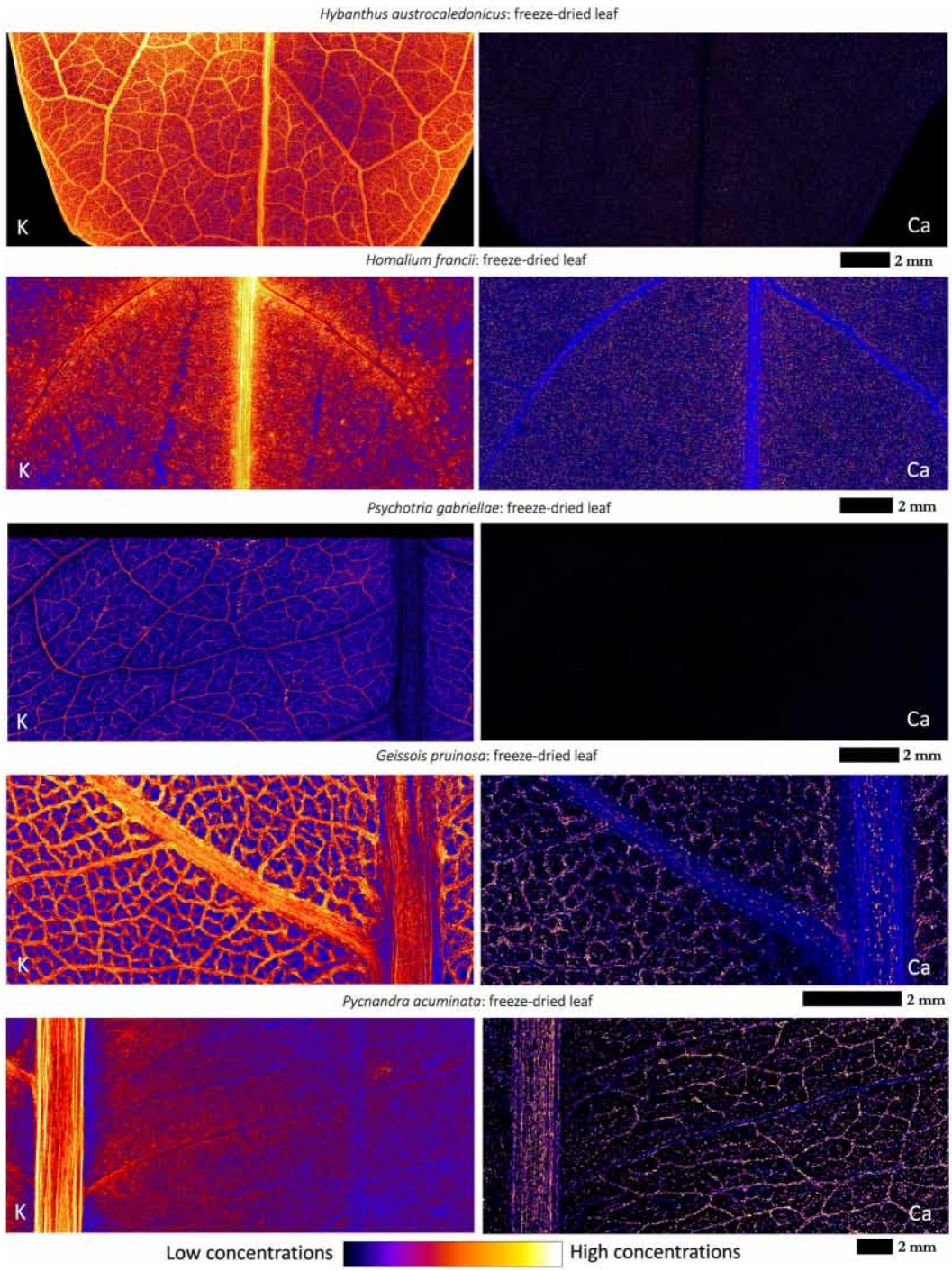

Fig. 4 Synchrotron μXRF maps of K and Ca of freeze-dried leaf portions of *Geissois pruinosa* var. *pruinosa*, *Psychotria gabriellae*, *Homalium francii*, *Hybanthus austrocaledonicus* and *Pycnandra acuminata*. The maps (w × h) measure 21.65 × 2.65 mm at 11 μm resolution with 10 ms dwell (*Hybanthus)*, 17.85 × 10.29 mm at 17 μm resolution with 10 ms dwell (*Homalium*), 23.27 × 7.39 mm at 10 μm resolution with 8 ms dwell (*Psychotria*), 11.91 × 16.63 mm at 10 μm resolution with 8 ms dwell (*Geissois*), and 11.91 × 17.52 mm at 10 μm resolution with 8 ms dwell (*Pycnandra*). Maps were cropped to fit figure panels

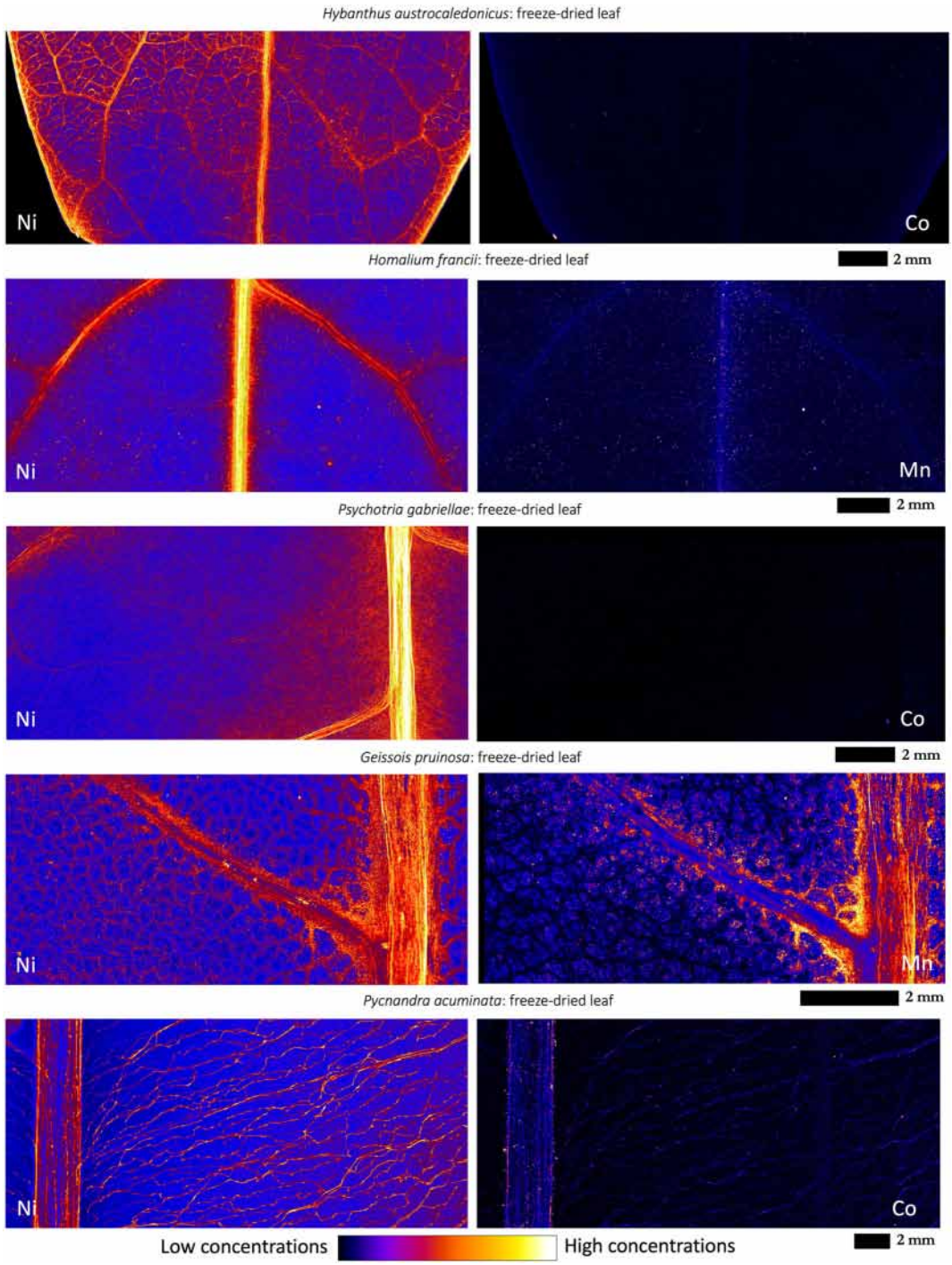

Fig. 5 Synchrotron μXRF maps of Ni, Co and/or Mn of freeze-dried leaf portions of *Geissois pruinosa* var. *pruinosa*, *Psychotria gabriellae*, *Homalium francii*, *Hybanthus austrocaledonicus* and *Pycnandra acuminata*. The maps (w × h) measure 21.65 × 2.65 mm at 11 μm resolution with 10 ms dwell (*Hybanthus)*, 17.85 × 10.29 mm at 17 μm resolution with 10 ms dwell (*Homalium*), 23.27 × 7.39 mm at 10 μm resolution with 8 ms dwell (*Psychotria*), 16.63 × 11.91 mm at 10 μm resolution with 8 ms dwell (*Geissois*), and 17.52 × 11.91 mm at 10 μm resolution with 8 ms dwell (*Pycnandra*). Maps were cropped to fit figure panels

lesser extent, this was also true for the secondary veins that are slightly thicker than the rest of the leaf blade. While Ni concentrations appeared to be very high in the midribs of *P. gabriellae* and *P. acuminata,* the cross sections (Fig. 7) revealed that Ni is in fact equally distributed in the epidermis of midrib and lamina.

Comparison of fresh/live leaves and freeze-dried leaf fragments

There appeared to be differences in the leaf K distribution of *G. pruinosa* var. *pruinosa* between freeze-dried and fresh material (Figs. 4 and 6). In freeze-dried material, K was mainly distributed in the vascular system of the leaf in the mid-rib and secondary veins. In the fresh leaf, it seemed to be absent from all vascular tissues and concentrated in cell clusters in the leaf lamina. With *P. gabriellae*, K in fresh samples was higher in the midrib, whereas it was mostly located in secondary veins and almost absent from the mid-rib in freeze-dried leaves. The distribution of Ni was generally similar (higher concentration in the mid-rib) in fresh and freeze-dried material for both species.

Elemental distribution in leaf midribs As the concentrations of all elements were apparently higher in the leaf midrib (but refer to earlier notes about the effect of sample thickness on XRF signal), a more detailed scan of these tissues was undertaken on cross-sectioned fresh material for two species (*P. gabriellae* and *P. acuminata*, Fig. 7). In *P. gabriellae*, K was present at high concentrations in all the tissues except in the epidermis. Potassium appeared to be located also in the vacuoles of most of the cells. In *P. acuminata*, K was also present in high concentration throughout the midrib, and was particularly rich in the parenchyma, K concentrations were much lower in the vascular system and almost depleted in the sclerenchyma surrounding vascular bundle.

Calcium was much less concentrated in midrib of both species. In *P. gabriellae* it appeared as small localised patches principally distributed in the parenchyma. These patches were Ca-oxalate crystals. In *P. acuminata*, Ca seemed to be only present in the adaxial epidermis of the midrib and not anywhere else. Nickel and Mn seemed to be clearly co-localised in the epidermis of both species. In *P. gabriellae*, both abaxial and adaxial epidermal cell layers contained the highest concentrations of both elements with Mn concentrations higher in the leaf blade epidermal tissues. However, in *P. acuminata*, only the adaxial epidermis had the highest Ni concentrations while Mn concentrations were intermediate to high in both epidermal tissues. In this species, a few hotspots with very high Ni concentrations also appeared in parenchyma and collenchyma (Fig. 7).

Elemental distribution in leaf petioles Petiole sections were examined as fresh samples for *G. pruinosa* var. *pruinosa*, *P. gabriellae* and *P. acuminata* and as freeze-dried samples for *H. francii* (Figs. 8 and 9). In all species K concentration was high in the cortex and phloem but occurred in much lower concentration in the xylem (Fig. 8). However, in *P. gabriellae* and *P. acuminata*, high K concentrations were notable in xylem rays. K concentration in the epidermis varied between species, with particularly high concentrations in *G. pruinosa* var. *pruinosa*. Calcium distribution was similar to K, but with lower concentrations in addition to low concentrations of Ca in the epidermal cells. Note that Ca appeared as small crystalline features likely in the form of Ca-oxalate.

Nickel in *G. pruinosa* var. *pruinosa* and *P. gabriellae* was located in the epidermis of the petiole with lower, but non-negligible, concentrations in the outer cortex of *P. gabriellae* (Fig. 9). In *H. francii*, the reverse was observed, and Ni was mostly concentrated in the inner part (parenchyma) and absent from the epidermis and the vascular bundle. In *P. acuminata*, a few large patches of high Ni concentration occurred randomly in the parenchyma, and small, but more regular, patches were observed in the adaxial epidermis of the petiole (the flatter part in the two sections). These large Ni patches were interpreted as leaking laticifers after sectioning of the fresh petiole. In *H. francii*, Zn was located in similar areas as Ni but at lower concentrations. Manganese in *G. pruinosa* var. *pruinosa* and *P. gabriellae* was only concentrated in the epidermis of the petiole.

Elemental distribution in fresh stem sections of Psychotria gabriellae In stem sections, the K concentrations were highest in the epidermis and progressively decreased towards the vascular tissues (Fig. 10). High concentrations, though much lower than in the epidermis, were also found in phloem tissues, pith and in the inner part of xylem tissues. Calcium was ubiquitous in the stem as localised Ca-oxalate deposits, except in the xylem tissues. The distribution pattern of Ni was clearly similar to that of K in stems, and Ni was even more pronouncedly enriched in the epidermal cell layer than K.

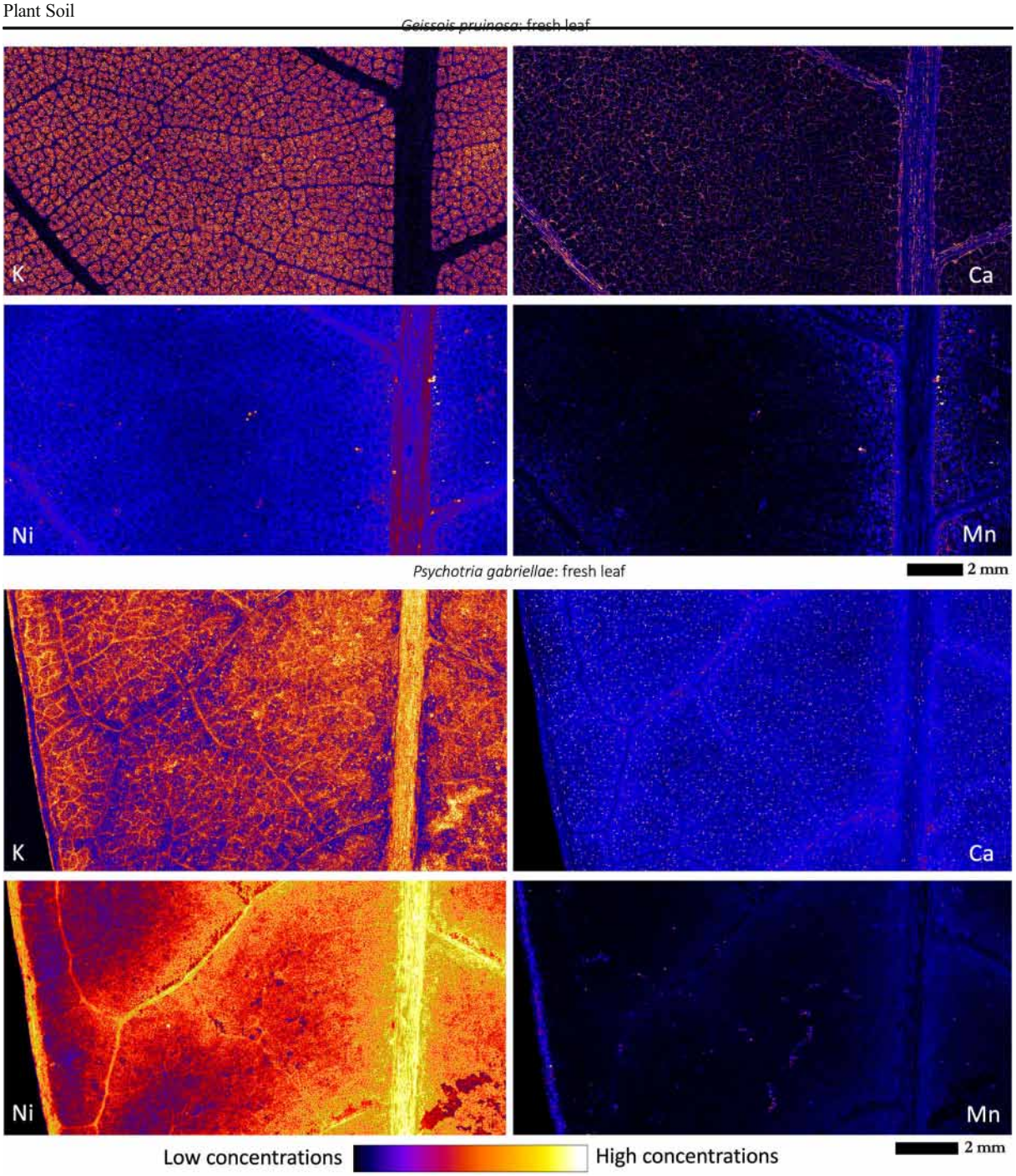

Fig. 6 Synchrotron μXRF maps of K, Ca, Ni and Mn of fresh leaf portions of *Geissois pruinosa* var. *pruinosa*, and *Psychotria gabriellae*. The maps (w × h) measure 29.39 × 9.15 mm at 8 μm resolution with 17 ms dwell (*Geissois*) and 16.2 × 12.3 mm at 15 μm resolution with 10 ms dwell (*Psychotria*). Maps were cropped to fit figure panels

Cell-level elemental distribution in Psychotria gabriellae High-resolution scans (0.5 μm) of a fresh/live hand-cut leaf blade of *P. gabriellae* were obtained (Fig. 11). The abaxial epidermis of this species contains two layers of large cells whereas the adaxial epidermis had only one layer (Fig. 11). Potassium was enriched in the mesophyll and highly enriched in the vacuoles of the abaxial epidermal

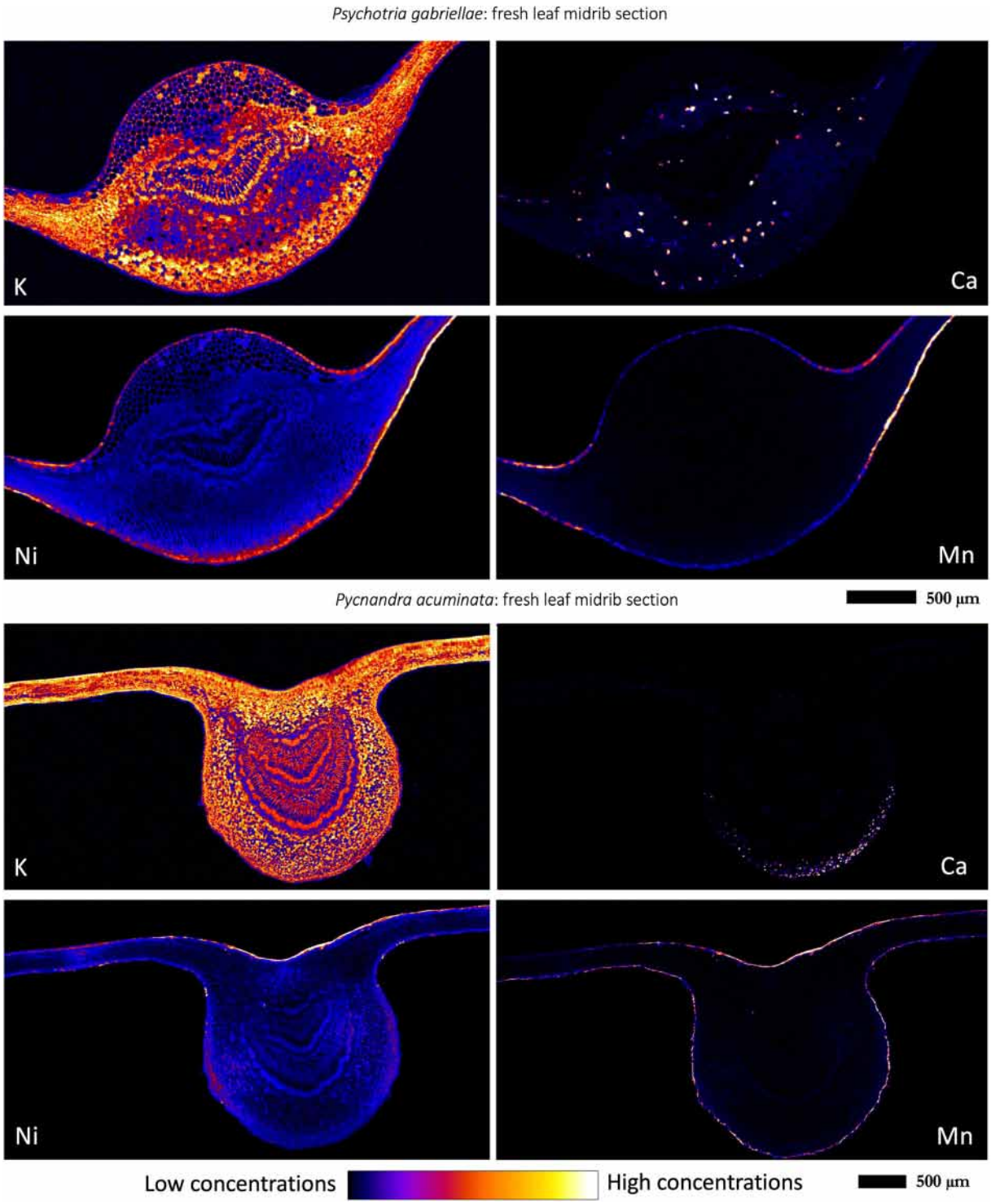

Fig. 7 Synchrotron µXRF maps of K, Ca, Ni and Mn of fresh leaf midrib portions of *Psychotria gabriellae* and *Pycnandra acuminata*. The maps (w × h) measure 3.49 × 2.12 mm at 8 µm resolution with 10 ms dwell *(Psychotria)* and 7.4 × 2.8 mm at 6 µm resolution with 8 ms dwell *(Pycnandra)*. Maps were cropped to fit figure panels

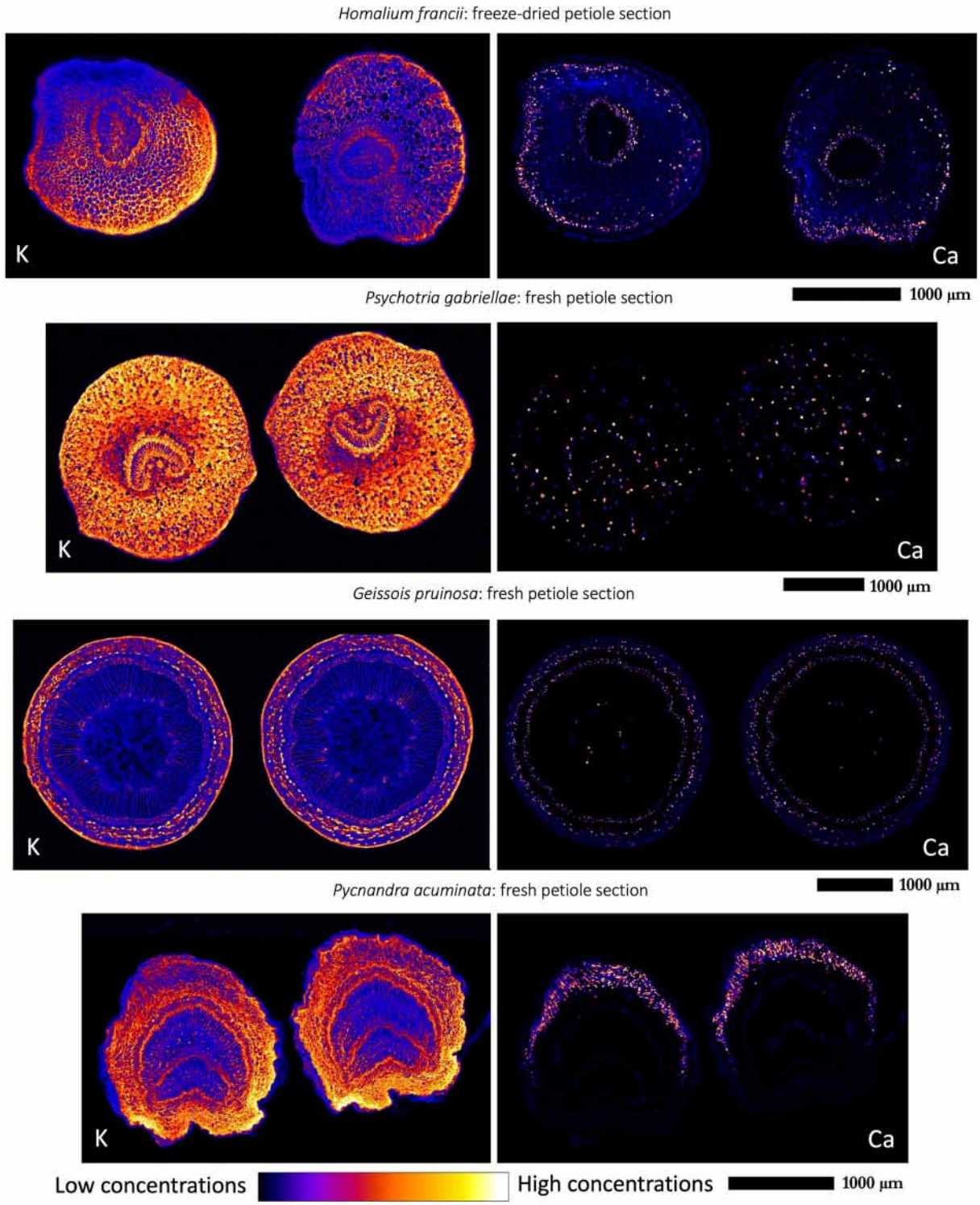

Fig. 8 Synchrotron µXRF maps of K and Ca of freeze-dried petiole portions of *Homalium francii*; and of fresh petioles portions of *Psychotria gabriellae, Geissois pruinosa* var. *pruinosa* and *Pycnandra acuminata*. The maps (w × h) measure 4.49 × 2.28 mm at 5 µm resolution with 10 ms dwell (*Homalium*), 5.5 × 3.08 mm at 8 µm resolution with 8 ms dwell (*Psychotria*), 6.3 × 5.68 mm at 7 µm resolution with 8 ms dwell (*Geissois*), and 3.9 × 2.35 mm at 5 µm resolution with 8 ms dwell (*Pycnandra*). Maps were cropped to fit figure panels

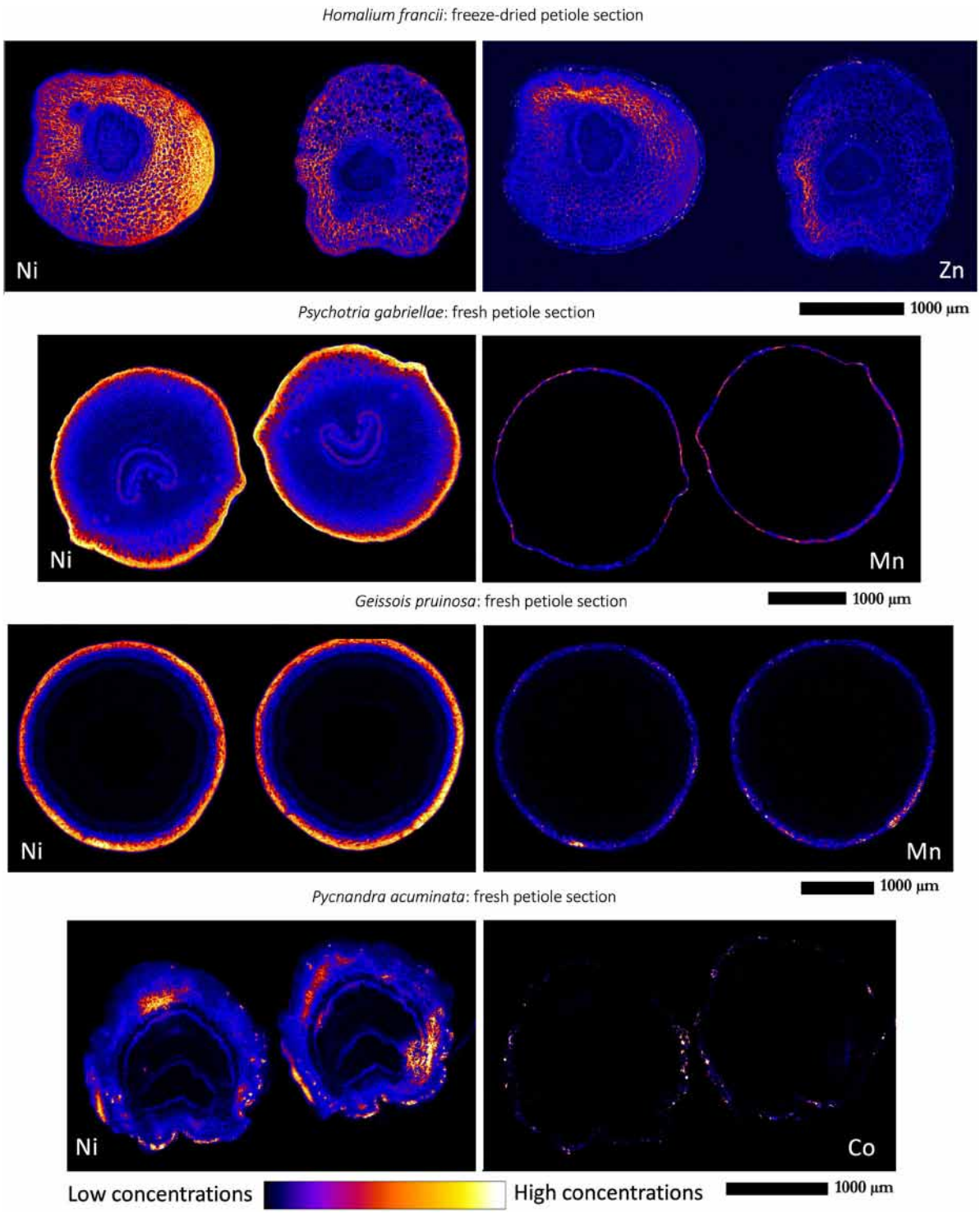

Fig. 9 Synchrotron µXRF maps of Ni and Zn, of freeze-dried petiole portions of *Homalium francii*; and Ni and Mn or Co of fresh petioles portions of *Psychotria gabriellae, Geissois pruinosa* var. *pruinosa* and *Pycnandra acuminata*. The maps (w × h) measure 4.49 × 2.28 mm at 5 µm resolution with 10 ms dwell (*Homalium*), 5.5 × 3.08 mm at 8 µm resolution with 8 ms dwell (*Psychotria*), 6.3 × 5.68 mm at 7 µm resolution with 8 ms dwell (*Geissois*), and 3.9 × 2.35 mm at 5 µm resolution with 8 ms dwell (*Pycnandra*). Maps were cropped to fit figure panels

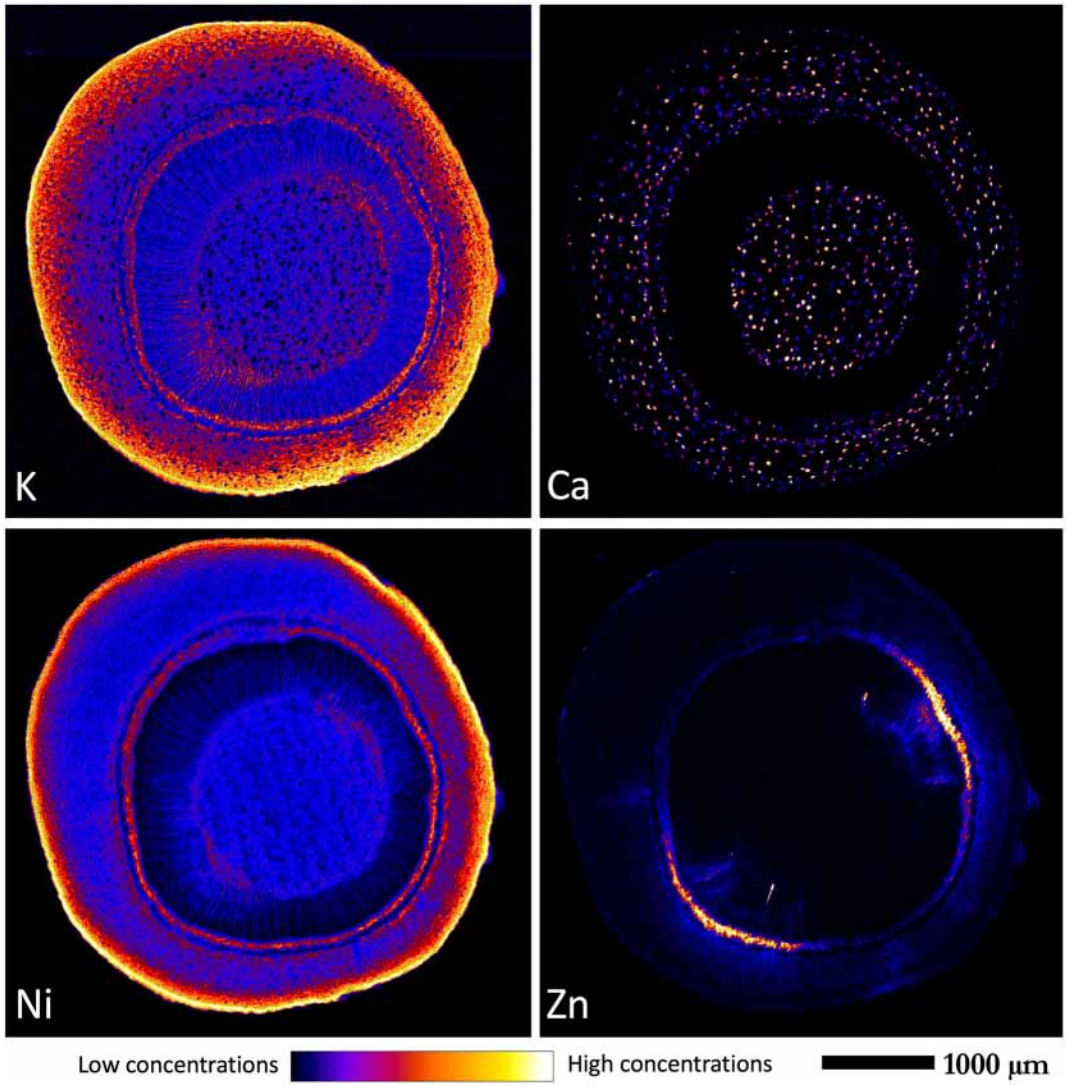

Fig. 10 Synchrotron µXRF maps of K, Ca, Ni and Zn, of fresh stem portions of *Psychotria gabriellae.* The maps (w × h) measure 4.7 × 4.58 mm at 8 µm resolution with 8 ms dwell. Maps were cropped to fit figure panels

cells. In contrast, Ca was strongly depleted in the vacuoles of these cells and only detectable in epidermal cell walls, but it formed localized Ca fibres (raphides of Ca-oxalate precipitates) in the spongy mesophyll. The distribution of Mn and Co was rather similar to each other and both elements were concentrated in the vacuoles of the adaxial epidermal cells. Zinc was slightly enriched in the spongy mesophyll. Nickel was extremely enriched in the vacuoles of the adaxial epidermal cells and to a lesser extent in the vacuoles of the outer layer of abaxial epidermal cells. It also appeared to be present in the apoplastic space between the inner layer cells of the abaxial epidermis. It was notably low in the palisade mesophyll.

Discussion

Soil-plant interactions and elemental uptake

While most Ni hyperaccumulators worldwide have been described from serpentinite soils (i.e. soils derived from serpentinite minerals characterised by very high Mg/Ca,

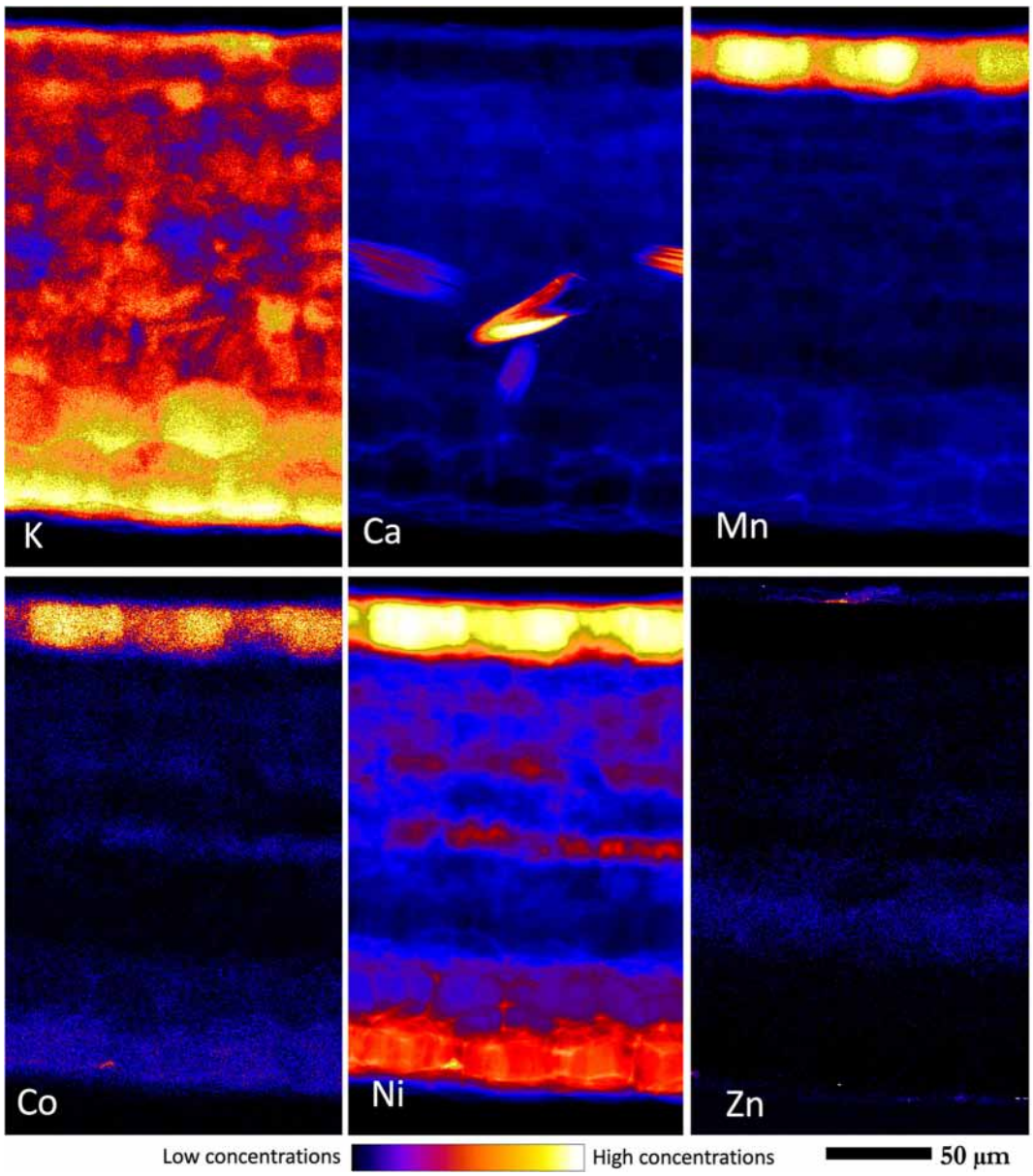

Fig. 11 Synchrotron µXRF maps of K, Ca, Mn, Co, Ni and Zn, of fresh leaf blade cross section of *Psychotria gabriellae.* The maps (w × h) measure 0.16 × 0.27 mm at 0.5 µm resolution with 15 ms dwell (*Psychotria*). Maps were cropped to fit figure panels

very low K and high pH, see Echevarria 2018), in New Caledonia hyperaccumulation also occurs on non-serpentinised peridotites. The high diversity of soils derived from ultramafic rocks is an important pedological feature of New Caledonia and ranges from magnesium-rich brown soils (e.g. Cambisols) to impoverished Fe-rich soils (e.g. Ferralsols) (Jaffré 1976; Isnard et al. 2016). All of the studied species reach the status of hypernickelophore (plant with >10 mg Ni g^{-1}); which may be partly explained by the high availability of Ni in all of the soil samples. This is mainly due to two processes; in the case of Monts des Koghis, soil erosion rejuvenates ultramafic properties of the ferralic material in the soils (van der Ent et al. 2018a), thus keeping exchangeable Mg and Ni at high concentrations with some contribution of moderate laterization. In the case of Rivière Bleue, the alluvial conditions and temporary waterlogging likely contribute to the dissolution of Ni-bearing Fe-

oxyhydroxides, thus releasing substantial amounts of available Ni (Antić-Mladenović et al. 2011). At Rivière Bleue, forest areas over peridotite humus-rich alluvium are Ni-rich and host the famous *P. acuminata* (Jaffré et al. 1976) and other hyperaccumulators (*H. austrocaledonicus, H. guillainii, P. gabriellae*) (Jaffré and Schmid 1974).

For major elements, four species out of five had notably high K concentrations reaching almost 10 mg K g^{-1} in the leaves except in *G. pruinosa* var. *pruinosa* (typically 2000 μg K g^{-1}). These concentrations are high for K-impoverished ultramafic soils (mean for K for 146 species in forest on ultramafic soils is 8.6 mg K g^{-1}), compared to plants growing on non-ultramafic soils (Jaffré 1980). The low Ca concentrations in the soil and low Ca/Mg quotients contribute to the edaphic stresses on ultramafic soils (Proctor 2003). In New Caledonia, exchangeable Ca^{2+} are very low, while Mg concentration are extremely high leading to very low Ca/Mg quotients on serpentinites (Jaffré 1976) and also on peridotites in this study. The Ca/Mg quotient in the leaves of all five species is high and close to 1 (with the exception of *H. austrocaledonicus*). The ability for preferential Ca over Mg uptake is characteristic for many ultramafic species (Brady et al. 2005; Brearley 2005), including Ni hyperaccumulators (Bani et al. 2007; van der Ent et al. 2018a).

Potassium and phosphorus are the most limiting nutrients in tropical ultramafic soils (Proctor 2003) where they have been leached or strongly bound to Fe oxides. Nickel hyperaccumulators efficiently take up these elements and significantly contribute to their biogeochemical cycling in ultramafic soils (Echevarria 2018). The association between Ni and nutrient assimilation remain unknown, though it has been suggested that extensive uptake of Ni is the result of root foraging for essential nutrients that are depleted in the soils. Another explanation is that Ni accumulation slows down plant development leading to stunted habit and greater uptake/accumulation of nutrients (Brooks et al. 1974). Sulphate is typically the dominant anion in ferralic ultramafic soils; therefore, it is not surprising that it is co-accumulated where cations are highly accumulated within the plant to ensure ionic balance.

In the case of Co, the foliar concentrations are sometimes high and associated with a high DTPA-Co/DTPA-Ni quotient in the soil. The Co availability is probably also enhanced during temporary reduction events in the alluvial soils from Rivière Bleue (where four out the five studied species were sampled). Similar results have been reported for a tropical Ni-Co hyperaccumulator plant (*Glochidion* cf. *sericeum*) from Borneo where unusually high Co uptake is linked to temporary waterlogged ultramafic soils (van der Ent et al. 2018c).

Latex of *Pycnandra acuminata*

Citrate is the main chelating agent of Ni in the latex of *P. acuminata* (Lee et al. 1978; Schaumlöffel et al. 2003; Callahan et al. 2008). However, citrate complexes have much higher stability constants (log K_1 values) with trivalent ions such as Al than with Ni, typical values for 1:1 complexes are reported to be 10.2, 4.8 and 4.5 for Al, Ni and Zn respectively (more than 10^5 times more stable than the Ni-citrate complex) (Martell et al. 2004; Cardiano et al. 2017). This may explain why we observed such high Al concentrations in the latex despite the low availability of soil Al. Zinc, which is more available than Al, was also high in the latex because it has a stability constant similar to Ni. High Al uptake and transfer by laticifers, while in low concentrations in branches, fruits and seeds, is possibly an indication that this network loads metals including Ni from the root up to all other plant parts independently from the vascular system (van der Ent et al. unpublished).

Effects of freeze-drying on elemental distribution

Scattering of X-rays by water reduces the signal from fresh hydrated samples (live samples) and this effect is more pronounced with low fluorescence energy (e.g. K). In contrast, freeze-drying increases the apparent concentration of an element by removing the solute and reducing X-ray scatter due to the absence of water. Calcium is present as Ca-rich deposits, presumably Ca-oxalate crystals (Franceschi and Nakata 2005), and as a consequence is not impacted by the water loss during freeze-drying. Given that K is the most mobile cation in plant tissues, it is likely to be more affected by the movement of water upon freeze-drying. There are several lines of evidence that show that freeze-drying does modify the distribution of elements at the micro-scale (Tylko et al. 2006; Wang et al. 2013). This study is the first to report extensive μXRF observations of fresh plant samples allowing for the analysis of larger surfaces than is possible for frozen-hydrated samples which need to be constantly maintained under a cold stream of N_2 gas (typically able to keep a sample area < 2 mm diameter wide frozen).

Patterns of Ni hyperaccumulation and other elements

The tissue-level and cellular-level distribution of Ni in the epidermal cells in *P. gabriellae, H. austrocaledonicus,* and *H. francii* conforms with the majority of studied Ni hyperaccumulator plant species globally, including (temperate) herbaceous species (see e.g. Broadhurst et al. 2004) and (tropical) woody plants (see van der Ent et al. 2017a, 2017b). However, two of the studied species (*G. pruinosa* var. *pruinosa* and *P. acuminata*) have distinctive patterns in their Ni tissue-level distribution from what has been observed so far in other species. *Geissois pruinosa* var. *pruinosa* accumulates high Ni, but much less potassium than all the other species (extremely high foliar K is a general feature among many Ni hyperaccumulators globally). In fact, K and Ni appear to have inverse foliar distribution in *G. pruinosa* var. *pruinosa* whereas they typically co-accumulate in other species (e.g. *P. gabriellae*).

Nickel is associated in tissues adjacent to vascular bundles in the epidermal tissues (and/or cortex); within vacuoles and apoplastic space in cell walls. When there is a lower Ni concentration it is only seen in the cell walls, but if there is a higher concentration it is observed in both the cell walls and in the vacuoles. That could mean that the preferred localisation for Ni storage is in the apoplastic space, only the extreme levels of hyperaccumulation would require active uploading into the vacuoles. The local distributions of Mn and Co are usually identical to that of Ni, inferring that co-accumulation could be due to the same transport pathways. However, the distribution of Zn is dissimilar to Ni, except for in *P. gabriellae*, and this mirrors the findings in the tropical Ni-Zn hyperaccumulator *Dichapetalum gelonioides* (Nkrumah et al. 2018).

Conclusions

Many tropical hyperaccumulator species have extraordinarily high Ca concentrations compared to prevailing soils concentrations (van der Ent and Mulligan 2015). Correlations between Ca and Ni have been reported in the leaves of *Hybanthus floribundus* from Australia (Farago and Mahmoud 1983). Here we report high Ca concentration in leaves, branches and bark, probably associated with calcium oxalate crystals deposited in the epidermis and the cortex (and in the pith in *P. gabriellae*). Calcium oxalate formation is a general mechanism for regulating bulk-free Ca^{2+} level in tissues and organs. It can also have a support function when located in the sclerenchyma. For *P. acuminata*, the high Ca contents in the abaxial cortex of petioles and midribs suggests that it has a role in reinforcing the structure of these long petioles. In *P. acuminata*, Ca is present in vascular bundles, also probably as Ca-oxalate crystals, and acts as a component of their structures. Nickel and Ca are proxies for two different and disconnected networks in this plant, the former for laticifers and the latter for the vascular system.

The laticifers constitute an independent network of cells that operate in parallel to the vascular systems (xylem and phloem) and is the main sink for Ni. Although the epidermal layer of *P. acuminata* leaves has been reported to be rich in Ni (Perrier et al. 2004), the SEM-EDS used in that study only probed to a maximum depth of 5 μm and hence was unable to reveal laticifers buried in the tissues. Because it has a greater penetration depth (>1000 μm for hydrated biological samples) synchrotron μXRF using hard X-rays (incident energy 12 keV) allows direct observation of the unique distribution of Ni in *P. acuminata*. Nickel is mostly present in laticifers and transported throughout the whole tree from roots to leaves. The occurrence of these Ni-rich laticifers is a specific phenomenon that has not been visualized with μXRF in other species to date. Laticifers are impossible to section without their destruction because they are pressurized (Pickard 2008). Consequently, physical sectioning of laticifers causes them to expel their contents resulting in Ni spills. In order to visualise laticifers, non-destructive techniques such as synchrotron X-ray fluorescence tomography (μXRF-CT) are required (de Jonge and Vogt 2010; Lombi et al. 2011; van der Ent et al. 2017b).

Acknowledgements The authors thank the Province Sud de Nouvelle-Calédonie for permission to collect the plant material samples (permits 1503-2016/ARR/DENV and 1206-2018/ARR/DENV), and S. Palermo for access to Monts des Koghis. This research was undertaken at P06 at DESY, a member of the Helmholtz Association (HGF). We would like to thank Gerald Falkenberg for assistance with the experiments. The research leading to this result has been supported by the project CALIPSOplus under the Grant Agreement 730872 from the EU Framework Programme for Research and Innovation HORIZON 2020. A. van der Ent was the recipient of a Discovery Early Career Researcher Award (DE160100429) from the Australian Research Council. V. Gei was the recipient of an Australia Awards PhD Scholarship from the Australian Federal Government.

References

Adıgüzel N, Reeves RD (2012) Important serpentine areas of Turkey and distribution patterns of serpentine endemics and nickel accumulators. Bocconea 24:7–17

Andresen E, Peiter E, Küpper H (2018) Trace metal metabolism in plants. J Exp Bot 69(5):909–954

Antić-Mladenović S, Rinklebe J, Frohne T, Stärk H-J, Wennrich R, Tomić Z, Ličina V (2011) Impact of controlled redox conditions on nickel in a serpentine soil. J Soils Sediments 11(3):406–415

Bani A, Echevarria G, Sulçe S, Morel JL, Mullai A (2007) In-situ phytoextraction of Ni by a native population of *Alyssum murale* on an ultramafic site (Albania). Plant Soil 293(1–2): 79–89

Becquer T, Bourdon E, Pétard J (1995). Disponibilité du nickel le long d'une toposéquence de sols développés sur roches ultramafiques de Nouvelle-Calédonie. Comptes Rendus de l'Académie des Sciences Série 2a 321:585–592

Berazaín R, de la Fuente V, Rufo L, Rodríguez N, Amils R, Díez-Garretas B, Sánchez-Mata D, Asensi A (2007) Nickel localization in tissues of different hyperaccumulator species of Euphorbiaceae from ultramafic areas of Cuba. Plant Soil 293(1):99–106

Bhatia NP, Orlic I, Siegele R, Ashwath N, Baker AJM, Walsh KB (2003) Elemental mapping using PIXE shows the main pathway of nickel movement is principally symplastic within the fruit of the hyperaccumulator *Stackhousia tryonii*. New Phytol 160:479–448

Bhatia NP, Walsh KB, Orlic I, Siegele R, Ashwath N, Baker AJM (2004) Studies on spatial distribution of nickel in leaves and stems of the metal hyperaccumulator *Stackhousia tryonii* bailey using nuclear microprobe (micro-PIXE) and EDXS techniques. Funct Plant Biol 31(11):1061–1074

Bidwell SD, Crawford SA, Woodrow IE, Sommer Knudsen J, Marshall AT (2004) Subcellular localization of Ni in the hyperaccumulator, *Hybanthus floribundus* (Lindley) F. Muell. Plant Cell Environ 27(6):705–716

Brady KU, Kruckeberg AR, Bradshaw HD Jr (2005) Evolutionary ecology of plant adaptation to serpentine soils. Annu Rev Ecol Evol Syst 36:243–266

Brearley F (2005) Nutrient limitation in a Malaysian ultramafic soil. J Trop For Sci 17(4):596–609

Broadhurst CL, Chaney RL, Angle JS, Erbe EF, Maugel TK (2004) Nickel localization and response to increasing Ni soil levels in leaves of the Ni hyperaccumulator *Alyssum murale*. Plant Soil 265:225–242

Broadhurst CL, Tappero RV, Maugel TK, Erbe EF, Sparks DL, Chaney RL (2009) Interaction of nickel and manganese in accumulation and localization in leaves of the Ni hyperaccumulators *Alyssum murale* and *Alyssum corsicum*. Plant Soil 314(1/2):35–48

Brooks RR, Robinson BH (1998) The potential use of hyperaccumulators and other plants for phytomining. In: Brooks RR (ed) Plants that hyperaccumulate heavy metals. CAB International, Wallingford, Oxon, pp 327–356

Brooks RR, Lee J, Jaffré T (1974) Some New Zealand and New Caledonia plant accumulators of nickel. J Ecol 62:493–499

Brooks RR, Morrison RS, Reeves RDR, Dudley TRT, Akman YY (1979) Hyperaccumulation of nickel by *Alyssum* Linnaeus (Cruciferae). Proceedings of the Royal Society of London. Series B 203:387–403

Brooks RR, Chambers MF, Nicks LJ, Robinson BH (1998) Phytomining. Trends Plant Sci 3(9):359–362

Callahan DL, Roessner U, Dumontet V, Perrier N, Wedd AG, O'Hair RAJ, Baker AJM, Kolev SD (2008) LC–MS and GC–MS metabolite profiling of nickel(II) complexes in the latex of the nickel-hyperaccumulating tree *Sebertia acuminata* and identification of methylated aldaric acid as a new nickel(II) ligand. Phytochemistry 69:240–251

Cardiano P, Cigala RM, Crea F, Giacobello F, Giuffre O, Irto A, Lando G, Sammartano (2017) Sequestration of aluminium(III) by different natural and synthetic organic and inorganic ligands in aqueous solution. Chemosphere 186:535–545

Chaney RL (1983) Potential effects of waste constituents on the food chain. In: Parr JF, Marsh PB, Kla JM (eds) Land treatment of hazardous wastes. Park Ridge, NJ, Noyes Data Corp, pp 152–240

Chaney RL, Angle JS, Broadhurst CL, Peters CA, Tappero RV, Sparks DL (2007) Improved understanding of hyperaccumulation yields commercial phytoextraction and phytomining technologies. J Environ Qual 36(5):1429–1443

de Jonge MD, Vogt S (2010) Hard X-ray fluorescence tomography-an emerging tool for structural visualization. Curr Opin Struct Biol 20:606–614

Echevarria G (2018) Genesis and behaviour of ultramafic soils and consequences for nickel biogeochemistry. In: van der Ent A, Echevarria G, Baker AJM, Morel JL (eds) Agromining: Farming for metals: extracting unconventional resources using plants: mineral resources reviews series. Springer International Publishing, Cham, pp 135–156

Echevarria G, Morel J, Fardeau J, Leclerc-Cessac E (1998) Assessment of phytoavailability of nickel in soils. J Environ Qual 27(5):1064–1070

Echevarria G, Massoura ST, Sterckeman T, Becquer T, Schwartz C, Morel JL (2006) Assessment and control of the bioavailability of nickel in soils. Environ Toxicol Chem 25(3):643–651

Erskine PD, Lee G, Fogliani B, L'Huillier L, McCoy S (2018) Incorporating Hyperaccumulator plants into mine rehabilitation in the Asia-Pacific region. In: van der Ent A, Echevarria G, AJM B, Morel JL (eds) Agromining: extracting unconventional resources from plants, Mineral resource reviews series. Springer international publishing, Cham, pp 117–133

Estrade N, Cloquet C, Echevarria G, Sterckeman T, Deng T, Tang Y, Morel JL (2015) Weathering and vegetation controls on nickel isotope fractionation in surface ultramafic environments (Albania). Earth Planet Sci Lett 423:24–35

Farago ME, Mahmoud IEDAW (1983) Plants that accumulate metals (part VI): further studies of an Australian nickel accumulating plant. Minerals and the Environment 5(4):113–121

Franceschi VR, Nakata PA (2005) Calcium oxalate in plants: formation and function. Annu Rev Plant Biol 56:41–71

Gei V, Erskine PD, Harris HH, Echevarria G, Mesjasz-Przybyłowicz J, Barnabas AD, Przybyłowicz WJ, Kopittke PM, van der Ent A (2018) Tools for discovery of hyperaccumulator plant species and understanding their ecophysiology. In: van der Ent A, Echevarria G, AJM B, Morel

JL (eds) Agromining: Farming for Metals: Extracting Unconventional Resources Using Plants, Mineral resource reviews series. Springer international publishing, Cham, pp 117–133

Gei V, Isnard S, Erskine PD, Echevarria G, Fogliani B, Jaffré T, van der Ent A (2020) A systematic assessment of the occurrence of trace element hyperaccumulation in the flora of New Caledonia. Bot J Linn Soc 194(1):1–22

Groeber S, Przybyłowicz W, Echevarria G, Montarges-Pelletier E, Barnabas A, Mesjasz-Przybyłowicz J (2015) Fate of nickel and calcium in seedlings of the hyperaccumulator *Berkheya coddii* during germination. Biol Plant 59(3):560–569

Hopkins HCF, Pillon Y, Hoogland R (2014). Cunoniaceae; Flore de la Nouvelle-Calédonie, Vol 25 Muséum Paris, IRD Marseille 455pp

Isnard S, L'Huillier L, Rigault F, Jaffré T (2016) How did the ultramafic soils shape the flora of the new Caledonian hotspot? Plant Soil 403(1):53–76

Jaffré T (1976). Composition chimique et conditions de l'alimentation minérale des plantes sur roches ultrabasiques (Nouvelle Calédonie). Cah ORSTOM Sér Biol 11

Jaffré T (1980) Étude écologique du peuplement végétal des sol dérivés de roches ultrabasiques en Nouvelle Calédonie. Travaux et Documents de L'ORSTOM 124. Paris: ORSTOM

Jaffré T, Schmid M (1974) Ecophysiologie - Accumulation du nickel par une Rubiacée de Nouvelle-Calédonie, *Psychotria douarrei* (G. Beauvisage) Däniker. Comptes Rendus de l'Académie des Sciences, Paris 278:1727–1730

Jaffré T, Veillon JM (1990) Etude floristique et structurale de deux forêts denses humides sur roches ultrabasiques en Nouvelle-Calédonie. Adansonia 3–4:243–273

Jaffré T, Brooks RR, Lee J, Reeves RD (1976) *Sebertia acuminata*: a hyperaccumulator of nickel from New Caledonia. Science 193:579–580

Jaffré T, Brooks RR, Trow JM (1979) Hyperaccumulation of nickel by *Geissois* species. Plant Soil 51(1):157–161

Jaffré T, Pillon Y, Thomine S, Merlot S (2013) The metal hyperaccumulators from New Caledonia can broaden our understanding of nickel accumulation in plants. Front Plant Sci 4(279):1–7

Jaffré T, Reeves RD, Baker AJM, van der Ent A (2018) The discovery of nickel hyperaccumulation in the new Caledonian tree *Pycnandra acuminata*: 40 years on. New Phytol 218:397–400

Jones MWM, Kopittke PM, Casey L, Reinhardt J, Blamey FPC, van der Ent A (2019) Assessing radiation dose limits for X-ray fluorescence microscopy analysis of plant specimens. Ann bot 125(4):599–610

Kachenko AG, Singh B, Bhatia NP, Siegele R (2008) Quantitative elemental localisation in leaves and stems of nickel hyperaccumulating shrub *Hybanthus floribundus* var. *floribundus* using micro-PIXE spectroscopy. Nucl Instrum Methods Phys Res, Sect B 266(4):667–676

Kirkham R, Dunn PA, Kuczewski AJ, Siddons DP, Dodanwela R, Moorhead GF, Ryan CG, De Geronimo G, Beuttenmuller R, Pinelli D et al (2010) The Maia spectroscopy detector system: engineering for integrated pulse capture, low-latency scanning and real-time processing. AIP Conference Proceedings 1234(1):240–243

Krämer U (2010) Metal Hyperaccumulation in plants. Annu Rev Plant Biol 61(1):517–534

Krämer U, Talke IN, Hanikenne M (2007) Transition metal transport. FEBS Letters 581:2263–2272

Kukier U, Chaney RL (2001) Amelioration of nickel phytotoxicity in muck and mineral soils. J Environ Qual 30:1949–1960

Küpper H, Lombi E, Zhao FJ, Wieshammer G, McGrath SP (2001) Cellular compartmentation of nickel in the hyperaccumulators *Alyssum lesbiacum, Alyssum bertolonii* and *Thlaspi goesingense*. J Exp Bot 51:2291–2300

Lee J, Reeves RD, Brooks RR, Jaffré T (1978) The relation between nickel and citric acid in some nickel-accumulating plants. Phytochemistry 17:1033–1035

Lindsay WL, Norvell WA (1978) Development of a DTPA soil test for zinc, iron, manganese, and copper. Soil Sci Soc Am J 42:421–428

Lombi E, de Jonge MD, Donner E, Kopittke PM, Howard DL, Kirkham R, Ryan CG, Paterson D (2011) Fast X-ray fluorescence microtomography of hydrated biological samples. PLoS One 6:e20626–e20625

Losfeld G, Mathieu R, L'Huillier L, Fogliani B, Jaffré T, Grison C (2015a) Phytoextraction from mine spoils: insights from New Caledonia. Environ Sci Pollut Res 22(8):5608–5619

Losfeld G, L'Huillier L, Fogliani B, Jaffré T, Grison C (2015b) Mining in new Caledonia: environmental stakes and restoration opportunities. Environ Sci Pollut Res 22(8):5592–5607

Martell AE, Smith RM, Motekaitis RJ. (2004). NIST critically selected stability constants of metal complexes database, 8.0. National Institute of standard and technology, Garthersburg, MD

Massoura ST, Echevarria G, Leclerc-Cessac E, Morel JL (2005) Response of excluder, indicator, and hyperaccumulator plants to nickel availability in soils. Soil Research 42(8): 933–938

McNear DH, Peltier E, Everhart J, Chaney RL, Sutton S, Newville M, Rivers M, Sparks DL (2005) Application of quantitative fluorescence and absorption-edge computed microtomography to image metal compartmentalization in *Alyssum murale*. Environmental Science & Technology 39(7):2210–2218

Mesjasz-Przybyłowicz J, Balkwill K (1994) Proton microprobe and X-ray fluorescence investigations of nickel distribution in serpentine flora from South Africa. Nucl Instrum Methods Phys Res Sect B 89:208–212

Mesjasz-Przybyłowicz J, Balkwill K, Przybylowicz WJ, Annegarn HJ, Rama DBK (1996a) Similarity of nickel distribution in leaf tissue of two distantly related hyperaccumulating species. In: van der Maesen LJG, van der Burgt XM, van Medenbach de Rooy JM (eds) The Biodiversity of African Plants. Springer, Dordrecht, pp 331–335

Mesjasz-Przybyłowicz J, Przybyłowicz WJ, Prozesky VM, Pineda CA (1996b) Elemental distribution in a leaf of *Senecio coronatus*. Proceedings of the Microscopy Society of Southern Africa 26:68

Mesjasz-Przybyłowicz J, Przybyłowicz WJ, Prozesky VM (1997a). Nuclear microprobe investigation of Ni distribution in organs and cells of hyperaccumulating plants. In: 'The ecology of ultramafic and metalliferous areas': proceedings of the second international conference on serpentine ecology, pp. 223–224

Mesjasz-Przybyłowicz J, Przybyłowicz WJ, Prozesky VM, Pineda CA (1997b) Quantitative micro-PIXE comparison of elemental distribution in Ni-hyperaccumulating and non-accumulating genotypes of *Senecio coronatus*. Nucl Instrum Methods Phys Res Sect B 130(1-4):368–373

Mesjasz-Przybyłowicz J, Przybyłowicz WJ, Rama DB, Pineda CA (1997c) Elemental distribution in the Ni hyperaccumulator – *Senecio anomalochrous*. Proceedings of the Microscopy Society of Southern Africa 27:89

Mesjasz-Przybyłowicz J, Przybyłowicz WJ, Pineda CA (2001a) Nuclear microprobe studies of elemental distribution in apical leaves of the Ni hyperaccumulator *Berkheya coddii*. S Afr J Sci 97:591–592

Mesjasz-Przybyłowicz J, Przybyłowicz WJ, Rama D, Pineda CA (2001b) Elemental distribution in *Senecio anomalochrous*, a Ni hyperaccumulator from South Africa. S Afr J Sci 97:593–595

Mesjasz-Przybyłowicz J, Barnabas A, Przybyłowicz W (2007) Comparison of cytology and distribution of nickel in roots of Ni hyperaccumulating and non-hyperaccumulating genotypes of *Senecio coronatus*. Plant Soil 293:61–78

Mesjasz-Przybyłowicz J, Przybyłowicz W, Barnabas A, van der Ent A (2016) Extreme nickel hyperaccumulation in the vascular tracts of the tree *Phyllanthus balgooyi* from Borneo. New Phytol 209:1513–1526

Nkrumah P, van der Ent A, Echevarria G, Erskine PD (2018) Contrasting nickel and zinc hyperaccumulation in subspecies of *Dichapetalum gelonioides* from Southeast Asia. Sci Rep 8: 9659

Paul ALD, Gei V, Isnard S, Fogliani B, Echevarria G, Erskine PD, Jaffré T, Munzinger J, van der Ent A (2020) Exceptional phloem nickel in *Hybanthus austrocaledonicus* (Violaceae) from New Caledonia. Ann Bot In Press. https://doi.org/10.1093/aob/mcaa112

Perrier N, Colin F, Jaffré T, Ambrosi J-P, Rose J, Bottero J-Y (2004) Nickel speciation in *Sebertia acuminata*, a plant growing on a lateritic soil of New Caledonia. Compt Rendus Geosci 336(6):567–577

Pickard WF (2008) Laticifers and secretory ducts: two other tube systems in plants. New Phytol 177:877–888

Pollard AJ, Powell KD, Harper FA, Smith JAC (2002) The genetic basis of metal hyperaccumulation in plants. Crit Rev Plant Sci 21:539–566

Proctor J (2003) Vegetation and soil and plant chemistry on ultramafic rocks in the tropical Far East. Perspectives in Plant Ecology, Evolution and Systematics 6(1):105–124

Reeves RD (2003) Tropical hyperaccumulators of metals and their potential for phytoextraction. Plant Soil 249:57–65

Reeves RD, Baker AJM, Becquer T, Echevarria G, Miranda ZJG (2007) The flora and biogeochemistry of the ultramafic soils of Goiás state, Brazil. Plant Soil 293(1):107–119

Reeves RD, Baker AJM, Jaffré T, Erskine PD, Echevarria G, van der Ent A (2018a) A global database for hyperaccumulator plants of metal and metalloid trace elements. New Phytol 218:407–411

Reeves RD, van der Ent A, Baker AJM (2018b) Global distribution and ecology of hyperaccumulator plants. In: van der Ent A, Echevarria G, AJM B, Morel JL (eds) Agromining: extracting unconventional resources from plants, Mineral Resource Reviews series. Springer International Publishing, Cham, pp 75–92

Ryan C (2000) Quantitative trace element imaging using PIXE and the nuclear microprobe. Int J Imaging Syst Technol 11(4):219–230

Ryan C, Jamieson D (1993) Dynamic analysis: on-line quantitative PIXE microanalysis and its use in overlap-resolved elemental mapping. Nucl Instrum Methods Phys Res, Sect B 77(1–4):203–214

Ryan C, Cousens D, Sie S, Griffin W, Suter G, Clayton E (1990) Quantitative PIXE microanalysis of geological material; using the CSIRO proton microprobe. Nucl Instrum Methods Phys Res, Sect B 47(1):55–71

Ryan C, Etschmann B, Vogt S, Maser J, Harland C, Van Achterbergh E, Legnini D (2005) Nuclear microprobe–synchrotron synergy: towards integrated quantitative real-time elemental imaging using PIXE and SXRF. Nucl Instrum Methods Phys Res, Sect B 231(1–4):183–188

Ryan CG, Siddons DP, Kirkham R, Dunn PA, Kuczewski A, Moorhead G, De Geronimo G, Paterson DJ, de Jonge MD, Hough RM et al (2010) The new Maia detector system: methods for high definition trace element imaging of natural material. AIP Conference Proceedings 1221(1):9–17

Ryan C, Siddons D, Kirkham R, Li Z, De Jonge M, Paterson D, Kuczewski A, Howard D, Dunn P, Falkenberg G. et al. (2014) Maia X-ray fluorescence imaging: capturing detail in complex natural samples. Journal of Physics: Conference Series: IOP Publishing. 012002

Sagner S, Kneer R, Wanner G, Cosson J, Deus-Neumann B, Zenk M (1998) Hyperaccumulation, complexation and distribution of nickel in *Sebertia acuminata*. Phytochemistry 47:339–347

Schaumlöffel D, Ouerdane L, Bouyssiere B, Łobiński R (2003) Speciation analysis of nickel in the latex of a hyperaccumulating tree *Sebertia acuminata* by HPLC and CZE with ICP MS and electrospray MS-MS detection. J Anal At Spectrom 18:120–127

Seregin IV, Kozhevnikova AD (2006) Physiological role of nickel and its toxic effects on higher plants. Russ J Plant Physiol 53(2):257–277

Siddons D, Kirkham R, Ryan C, De Geronimo G, Dragone A, Kuczewski A, Li Z, Carini G, Pinelli D, Beuttenmuller R, et al. (2014). Maia X-ray microprobe detector array system. Journal of Physics: Conference Series: IOP Publishing 012001

Swenson U, Munzinger J (2010) Revision of *Pycnandra* subgenus *Sebertia* (Sapotaceae) and a generic key to the family in New Caledonia. Adansonia 32(2):239–249

Tappero R, Peltier E, Gräfe M, Heidel K, Ginder-Vogel M, Livi KJT, Rivers ML, Marcus MA, Chaney RL, Sparks DL (2007) Hyperaccumulator *Alyssum murale* relies on a different metal storage mechanism for cobalt than for nickel. New Phytol 175:641–654

Tylko G, Mesjasz-Przybyłowicz J, Przybyłowicz WJ (2006) X-ray microanalysis of biological material in the frozen-hydrated state by PIXE. Microsc Res Tech 70:55–68

van der Ent A, Mulligan DM (2015) Multi-element concentrations in plants parts and fluids of Malaysian nickel hyperaccumulator plants and some economic and ecological considerations. J Chem Ecol 41:396–408

van der Ent A, Baker AJM, Reeves RD, Pollard AJ, Schat H (2012) Hyperaccumulators of metal and metalloid trace elements: facts and fiction. Plant Soil 362(1):319–334

van der Ent A, Baker A, Van Balgooy M, Tjoa A (2013) Ultramafic nickel laterites in Indonesia (Sulawesi, Halmahera): mining, nickel hyperaccumulators and opportunities for phytomining. J Geochem Explor 128:72–79

van der Ent A, Baker AJM, Reeves RD, Chaney RL, Anderson CWN, Meech JA, Erskine PD, Simonnot M-O, Vaughan J, Morel JL, Echevarria G, Fogliani B, Rongliang Q, Mulligan DR (2015a) Agromining: farming for metals in the future? Environmental Science & Technology 49(8):4773–4780

van der Ent A, Erskine PD, Sumail S (2015b) Ecology of nickel hyperaccumulator plants from ultramafic soils in Sabah (Malaysia). Chemoecology 25(5):243–259

van der Ent A, Jaffré T, L'Huillier L, Gibson N, Reeves RD (2015c) The flora of ultramafic soils in the Australia-Pacific region: state of knowledge and research priorities. Aust J Bot 63(4):173–190

van der Ent A, Callahan DL, Noller BN, Mesjasz-Przybyłowicz J, Przybyłowicz WJ, Barnabas A, Harris HH (2017a) Nickel biopathways in tropical nickel hyperaccumulating trees from Sabah (Malaysia). Sci Rep 7:41861

van der Ent A, Przybyłowicz WJ, de Jonge MD, Harris HH, Ryan CG, Tylko G, Paterson DJ, Barnabas AD, Kopittke PM, Mesjasz-Przybyłowicz J (2017b) X-ray elemental mapping techniques for elucidating the ecophysiology of hyperaccumulator plants. New Phytol 218:432–452

van der Ent A, Cardace D, Tibbett M, Echevarria G (2018a) Ecological implications of pedogenesis and geochemistry of ultramafic soils in Kinabalu Park (Malaysia). Catena 160: 154–169

van der Ent A, Harris HH, Erskine PDEG (2018b) Simultaneous hyperaccumulation of nickel and cobalt in *Glochidion* cf. *sericeum* (Phyllanthaceae): elemental distribution and speciation. Sci Rep 8:9683

van der Ent A, Mulligan DR, Repin R, Erskine PD (2018c) Foliar elemental profiles in the ultramafic flora of Kinabalu Park (Sabah, Malaysia). Ecol Res 33(3):659–674

Wang YD, Mesjasz-Przybyłowicz J, Tylko G, Barnabas AD, Przybyłowicz WJ (2013) Micro-PIXE analyses of frozen-hydrated semi-thick biological sections. Nucl Instrum Methods Phys Res, Sect B 306:134–139